Petroleum Science 23 (2026) 3875–3891

Contents lists available at ScienceDirect

Petroleum Science

journal homepage: www.keaipublishing.com/en/journals/petroleum-science

Original Paper

Pore pressure control on multi-scale reservoir properties in deep and ultra-deep sandstones of the Cretaceous Bashijiqike Formation, Kuqa Depression, Tarim Basin, NW China

Yang Su [a,b], Jin Lai [a,b,*], Wen-Le Dang [b], Rong-Hu Zhang [c], Kai-Xun Zhang [d], Yi Xin [e,f], Xiang Shan [c], Yong Ai [e], Gui-Wen Wang [a,b]

[a] *State Key Laboratory of Petroleum Resources and Engineering, China University of Petroleum (Beijing), Beijing, 102249, China*
[b] *College of Geosciences, China University of Petroleum (Beijing), Beijing, 102249, China*
[c] *PetroChina Hangzhou Research Institute of Geology, Hangzhou, 310023, Zhejiang, China*
[d] *Institute of Geomechanics, Chinese Academy of Geological Sciences, Beijing, 100081, China*
[e] *Research Institute of Petroleum Exploration and Development, Tarim Oilfield Company, CNPC, Korla, 841000, Xinjiang, China*
[f] *CNPC Coalbed Methane Company, Beijing, 100011, China*

ARTICLE INFO

Article history:
Received 23 July 2025
Received in revised form
8 December 2025
Accepted 22 May 2026
Available online 28 May 2026

Edited by Xiu-Fang Hu

Keywords:
Pore pressure
Reservoir properties
Deep and ultra-deep
Pore structure
Stress
Kuqa Depression

ABSTRACT

Understanding the effects of pore pressure on multiscale reservoir properties in deep and ultra-deep sandstones is important for many geological processes. This study integrated core analysis, computed tomography (CT) scanning, petrography, and well logs to quantify the effects of pore pressure on multiscale reservoir properties of the Cretaceous Bashijiqike Formation in the Kuqa Depression, Tarim Basin, NW China. Pore pressure was measured from Modular Formation Dynamics Tester (MDT), and then Eaton's method, which incorporates sonic transit time and vertical effective stress, was used for pore pressure prediction. Image logs were used for fracture characterization including identification of fracture appearances and calculation of fracture aperture. The crossplot between pore pressure and core-measured porosity reveals that elevated pore pressure mechanically inhibits compaction-driven porosity loss and effectively maintains porosity during deep burial. A pore pressure coefficient higher than 1.75 is an important factor in maintaining matrix porosity as high as 6.0% at depths exceeding 6000 m. Correlation analysis of measured pore pressure coefficient and mechanical fracture aperture demonstrates that elevated pore pressure promotes the opening of natural fractures, and mechanical fracture aperture can reach 4.7 mm when the pore pressure coefficient is higher than 1.75. In addition, pore pressure has positive effects on microscopic pore structure, and increasing the pore pressure coefficient contributes to a higher pore throat radius. Coarse-grained and well-sorted sandstones with pore pressure coefficient higher than 1.75 contribute to a maximum pore throat radius (r_{max}) higher than 1.0 μm. A structural model synthesizing these findings reveals that overpressure compartments in the fore-thrust and back-thrust of fold-and-thrust belts are favorable for the openness of fractures and preservation of matrix porosity and pore structure. The quantitative relationships between pore pressure and multiscale reservoir properties provide a new and robust analog framework for reservoir quality prediction in other deep compressional basins.
© 2026 The Authors. Publishing services by Elsevier B.V. on behalf of KeAi Communications Co. Ltd. This is an open access article under the CC BY license (http://creativecommons.org/licenses/by/4.0/).

1. Introduction

Multi-scale petrophysical behaviors in deep and ultra-deep sandstones are critical to understanding how geological processes and reservoir conditions influence fluid flow and storage capacities at different scales (Barker and Takach, 1992; Lai et al., 2023; Laubach et al., 2023; Wang et al., 2023). Deep and ultra-deep sandstone reservoirs have become strategically vital for

* Corresponding author.
E-mail address: sisylaijin@163.com (J. Lai).
Peer review under the responsibility of China University of Petroleum (Beijing).

https://doi.org/10.1016/j.petsci.2026.05.038
1995-8226/© 2026 The Authors. Publishing services by Elsevier B.V. on behalf of KeAi Communications Co. Ltd. This is an open access article under the CC BY license (http://creativecommons.org/licenses/by/4.0/).

hydrocarbon exploration strategies due to their potential for plentiful unconventional resources (Barker and Takach, 1992; Laubach et al., 2023; Wang et al., 2023; Zeng et al., 2023). Deep strata are generally considered to be those at depths greater than 4500 m, while ultra-deep strata refer to the strata exceeding 6000 m (Zeng et al., 2023). Deeply and ultra-deeply buried rocks are subjected to prolonged geological processes at extreme temperatures (150–180 °C or higher), stress and high pore pressures, having significant influences on their reservoir properties at different scales (Becker et al., 2010; Hassanzadegan et al., 2014; Geng et al., 2017; Meyer et al., 2024; Zhao et al., 2025b). Deep and ultra-deep wells present complex theoretical and technical challenges in reservoir property evaluation of subsurface rocks (Dutton and Loucks, 2010; Bjørlykke, 2014; Lai et al., 2023; Laubach et al., 2023). The anomalously high porosity is in some cases retained in deep and ultra-deep sandstones, even with depth exceeding 8000 m, and this challenges conventional porosity-depth trends (Bloch et al., 2002; Guo et al., 2016a; Lai et al., 2017).

A growing consensus suggests the critical role of pore pressure in influencing the multi-scale reservoir properties of deep and ultra-deep sandstones through four mechanisms (Screaton et al., 2002; Becker et al., 2010; Guo et al., 2016a; Zeng et al., 2020; Nikolinakou et al., 2023): (1) primary porosity preservation where elevated pore pressure reduces vertical effective stress at grain-to-grain contacts, resulting porosity loss from burial depth (Hart et al., 1995; Osborne and Swarbrick, 1997; Screaton et al., 2002; Siggins and Dewhurst, 2003; Guo et al., 2016a; Stricker and Jones, 2018; Zeng et al., 2020; Nikolinakou et al., 2023); (2) secondary porosity enhancement through extended organic acid dissolution facilitated by overpressure-prolonged hydrocarbon generation windows (Hao et al., 2007; Xi et al., 2021); (3) promotion of the early-formed fractures' openness, influencing their opening rate and degree (Baghbanan and Jing, 2008; Becker et al., 2010; Wang et al., 2020a; Cao et al., 2021); (4) the comprehensive modification of the pore structure through the expansion and interconnection of existing pores (Liu et al., 2020; Mahanta et al., 2021).

Pore pressure, which is the pressure exerted by fluids in rock pore spaces on the solid matrix, is crucial for reservoir property evaluation (Zhang, 2011; Zhang et al., 2021). Pore pressure is analyzed through direct measurement by drill-stem tests and well logs, or through indirect estimation using geomechanical models and fluid inclusion analysis (Zhang, 2011; Najibi et al., 2017; Zhang et al., 2021). Overpressure (abnormally high fluid pressure exceeding hydrostatic pressure) can be generated by many mechanisms including compaction disequilibrium, tectonic compression, aquathermal pressuring, fluid release during dehydration reactions, hydrocarbon generation and thermal cracking of oil to gas (Guo et al., 2016b; Fan et al., 2021). The Kuqa Depression in Tarim Basin of NW China exhibits widespread overpressure (pressure coefficients up to 2.1) in deep and ultra-deep sandstones, which are mainly driven by tectonic compression and gas generation (Guo et al., 2016b; Wang et al., 2022).

Extensive research has examined the effects of pore pressure on petrophysical properties (porosity and permeability, pore structure and fracture) (Becker et al., 2010; Guo et al., 2016b; Fan et al., 2021). However, a comprehensive and quantitative understanding of how pore pressure influences the reservoir performances from macroscopic fractures to microscopic pore systems remains elusive. In particular, the quantitative links between in-situ stress, pore pressure, and microscopic pore structure have been underexplored. A diverse suite of data including direct pressure measurements (MDT), core analysis, CT scanning, petrography, and well logs, is utilized. As a result, quantitative correlations between pore pressure and multi-scale reservoir properties are established. Specifically, the role of overpressure in preserving matrix porosity is quantified. Secondly, the quantitative relationship between pore pressure and fracture aperture is determined. Thirdly, the impact of pore pressure on microscopic pore-throat connectivity is elucidated. Finally, by integrating these findings into a geological model of a fold-and-thrust belt, this study provides an overall framework for understanding the impact of pore pressure on reservoir properties in deep and ultra-deep sandstones.

Specifically, this study utilizes a large and diverse dataset from the Cretaceous Bashijiqike Formation to achieve the following objectives: (1) to quantitatively assess the relationship between pore pressure and preservation of matrix porosity; (2) to establish a quantitative link between pore pressure and fracture aperture; (3) to elucidate the impact of pore pressure on microscopic pore-throat connectivity; and (4) to integrate these multi-scale findings into a predictive geological model for reservoir quality distribution in a fold-and-thrust belt setting. The novelty of this work lies in its integrated, multi-scale and highly quantitative approach within a well-defined and constrained geological unit. This study provides an integrated and multi-scale approach to address these gaps between pore pressure and multiscale reservoir properties. The results are expected to serve as a valuable analog for similar basins worldwide.

2. Geological settings

The Kuqa Depression, situated at the northern margin of the Tarim Basin, NW China (Fig. 1(a) and (b)), constitutes a segment of a rejuvenated foreland basin (Lai et al., 2019; Li et al., 2024; Zhang et al., 2024; Zhao et al., 2025a). The region has experienced ongoing compressional stresses exerted by the Indian Plate's continuous northward movement and the progressive inversion of the South Tianshan thrust belt (Molnar and Tapponnier, 1975; Huang et al., 2006; Sun et al., 2017). This compressional regime has generated six NE–SW trending tectonic belts arranged sequentially from north to south: the Northern Monocline Belt, Kelasu Structural Belt, Baicheng Sag, Qiulitage Structural Belt, Yangxia Sag, and Southern Gentle Monocline Belt (Fig. 1(c)) (Ju et al., 2014; Sun et al., 2017; Yang et al., 2024a; Li et al., 2025).

The Kelasu Structural Belt, located in the northern Kuqa Depression, displays a complex deep structure influenced by surface and subsurface deformation, coupled with extensive salt tectonics (Wang et al., 2020b; Yang et al., 2024a) (Fig. 1(c)). A series of large gas fields have been discovered in the Kelasu Structural Belt, among them, the Bozi-Dabei Gas Field has huge gas reserves over 1.0×10^{12} m^3 (Fig. 1(d)). The main gas-producing intervals are the Cretaceous Bashijiqike Formation. The Bashijiqike Formation is stratigraphically divided into three members in ascending order: K_1bs^3, K_1bs^2 and K_1bs^1. In the Kuqa Depression, the thrust-fold belt hosts optimal hydrocarbon accumulation, with the Bashijiqike Formation constituting the principal gas-bearing reservoir. Regional uplift since the Late Cretaceous resulted in an unconformable contact between the Paleocene–Eocene Kumugeliemu Formation and the Lower Cretaceous strata (Yu et al., 2014). The deposition within the Kuqa Depression occurred in an oxygen-rich continental environment, characterized by alluvial fan, deltaic, and saline lacustrine depositional systems. The Cretaceous Bashijiqike Formation in the Bozi-Dabei Gas Field of the Kuqa Depression was deposited in a high-energy braided to fan-delta environment, and subaqueous distributary channels and river-mouth bar microfacies (fine- to medium-grained sandstones and conglomerates) are the dominant microfacies (Lai et al., 2017).

The petrophysical properties of the Bashijiqike Formation reservoirs are the comprehensive effects of a long and complex geological history. Fig. 2 provides a comprehensive display of the

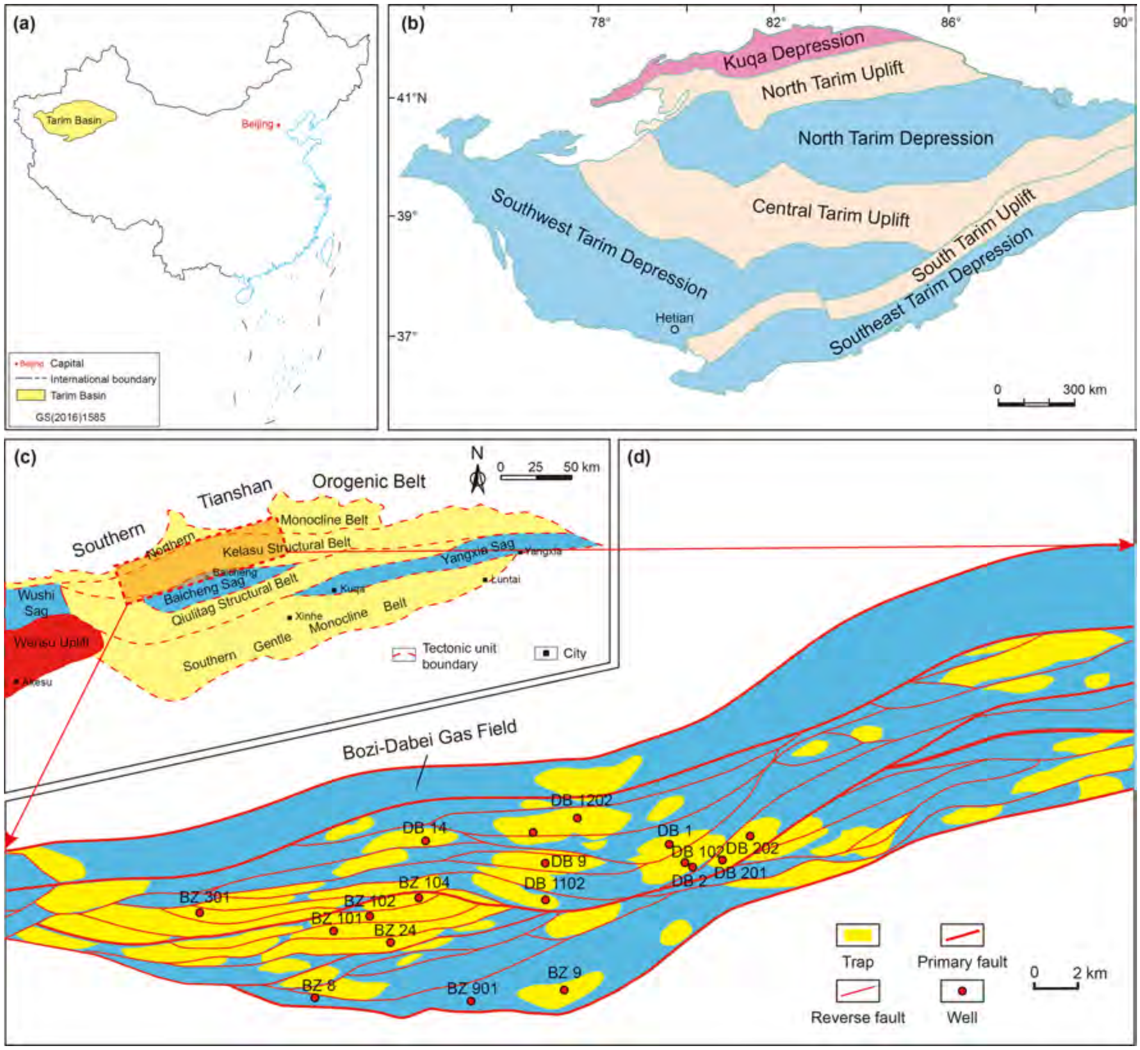

Fig. 1. Geological context of Bozi-Dabei Gas Field in the Kuqa Depression of the Tarim Basin, NW China (Lai et al., 2017; Yang et al., 2024b). **(a)** Location of the Tarim Basin; **(b)** major tectonic units within the Tarim Basin, with the Kuqa Depression highlighted at the northern margin; **(c)** tectonic map of the Kuqa Depression, showing the distribution of the six main NE–SW trending tectonic belts, including the Kelasu Structural Belt; **(d)** detailed tectonic map of the Bozi-Dabei Gas Field within the Kelasu Structural Belt, indicating the locations of key wells used in this study and the major fault systems.

synergistic evolution of the reservoir's burial history, pore pressure, and porosity since the Cretaceous in Kuqa Depression (Guo et al., 2016c; Zeng et al., 2020). The burial history model reveals two distinct phases (Fig. 2). The first phase, associated with the Yanshan Movement, involved relatively slow and shallow burial (Fig. 2(a)). This was followed by a second phase, beginning around 50 Ma with the Himalayan Movement, which led to rapid and deep burial exceeding 8000 m (Fig. 2) (Guo et al., 2016c; Zeng et al., 2020).

Since the Neogene (23–2.6 Ma), the Mesozoic–Cenozoic strata in the Kuqa Depression have experienced intense structural reworking. This tectonic activity coincides with the development of significant overpressure, with maximum pressure coefficients reaching 2.1 in both the Cretaceous and Eocene reservoirs (Guo et al., 2016b; Fan et al., 2021). The pore pressure coefficient evolution reconstructed by Guo et al. (2016c) also demonstrates that significant overpressure generation intensified within 5 Ma (Fig. 2(b)).

The primary mechanisms for overpressure generation include tectonic compression largely driven by the uplift of the Tianshan Mountains, as well as disequilibrium compaction and hydrocarbon generation (Zeng et al., 2010; Guo et al., 2016a; Fan et al., 2021). Furthermore, the presence of a regional salt seal has been essential in preserving these overpressures by effectively inhibiting fluid escape (Jia et al., 2002; Zeng et al., 2010; Guo et al., 2016b, 2016c).

3. Data and methods

Samples and data collected for this study are from a depth range of approximately 5000 m to 8100 m. Drilled core and plug samples were taken from the Cretaceous Bashijiqike Formation in the Wells BZ 104, DB 9, DB 902, BZ 17, etc. in the Kuqa Depression (Fig. 1(d)).

Schlumberger's Modular Formation Dynamics Tester (MDT) was deployed to establish hydraulic isolation between wellbore fluids and reservoir formations through advanced packer sealing technology. This wireline formation testing tool provides direct pore pressure measurements through real-time monitoring of stabilized pressure buildups, delivering critical data for reservoir compartmentalization analysis (Anderson et al., 2011).

Standard 10 cm diameter core specimens were retrieved from Cretaceous Bashijiqike sandstone intervals using rotary sidewall

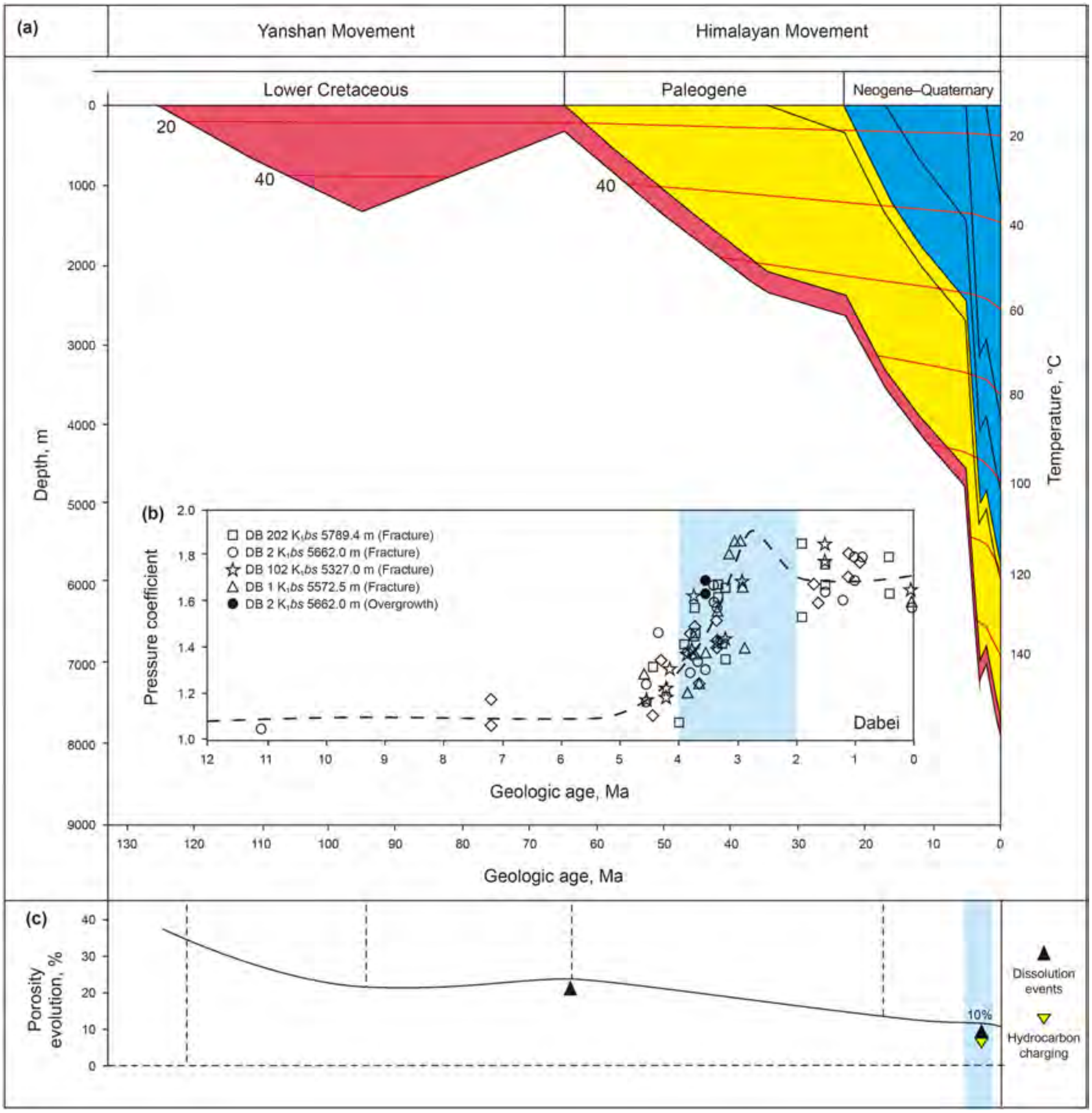

Fig. 2. Integrated diagram of burial history, pressure evolution, and porosity evolution for the reservoir in the Bozi-Dabei Gas Field in Kuqa Depression (Guo et al., 2016c; Zeng et al., 2020). **(a)** The burial and thermal history since the Lower Cretaceous, influenced by the Yanshan and Himalayan movements (Zeng et al., 2020); **(b)** evolution of the pore pressure coefficient (Guo et al., 2016c) showing significant overpressure generation (blue shaded region) since 5 Ma; **(c)** porosity evolution curve derived from diagenetic modeling and calibrated with present-day core data.

coring systems. Thin sections with a thickness of 30 μm were impregnated with blue-dye or red-dye resin to detect pore spaces for microscopic examination of the pore structure at the micro-scale. Permeability was quantified using a DX-07G gas permeability tester, while porosity was assessed with the Ultra-Pore 400 system.

The pore structure characteristics of the samples were quantitatively evaluated using a high-pressure mercury intrusion (HPMI) test. The intrusion and extrusion curves were recorded to analyze the connectivity and heterogeneity of the pore network. Key parameters, including total pore volume and median pore diameter, were derived from the cumulative mercury saturation data.

High-resolution borehole image logs (FMI-HD) provide a centimeter-scale characterization of fractures through 192-button resistivity mapping (Lai et al., 2022). The fracture aperture was calculated from FMI-HD borehole images. Fractures filled with conductive drilling mud appear as dark, sinusoidal features. The width of this conductive anomaly is proportional to the fracture's mechanical aperture. A standard algorithm based on the principles of Luthi and Souhaite (1990) was adopted to calculate the excess current flowing into the fracture to estimate its width. This log-derived mechanical aperture can be estimated by Eq. (1) and was then calibrated with available core data to ensure accuracy.

$$\mathrm{FVA} = aAR_{\mathrm{m}}^{b}R_{\mathrm{xo}}^{1-b} \tag{1}$$

where A represents the integrated additional current, m^2; R_{xo} is the resistivity of the invaded zone, Ω·m; R_{m} is the resistivity of the drilling mud, Ω·m; and a and b are coefficients specific to the imaging tool (Luthi and Souhaite, 1990).

The petrophysical properties of the reservoir rock were evaluated under varying confining pressures and pore fluid pressures. Cylindrical specimens with nominal dimensions of 25 mm in diameter and 50 mm in height (height-to-diameter ratio ≈ 2.0)

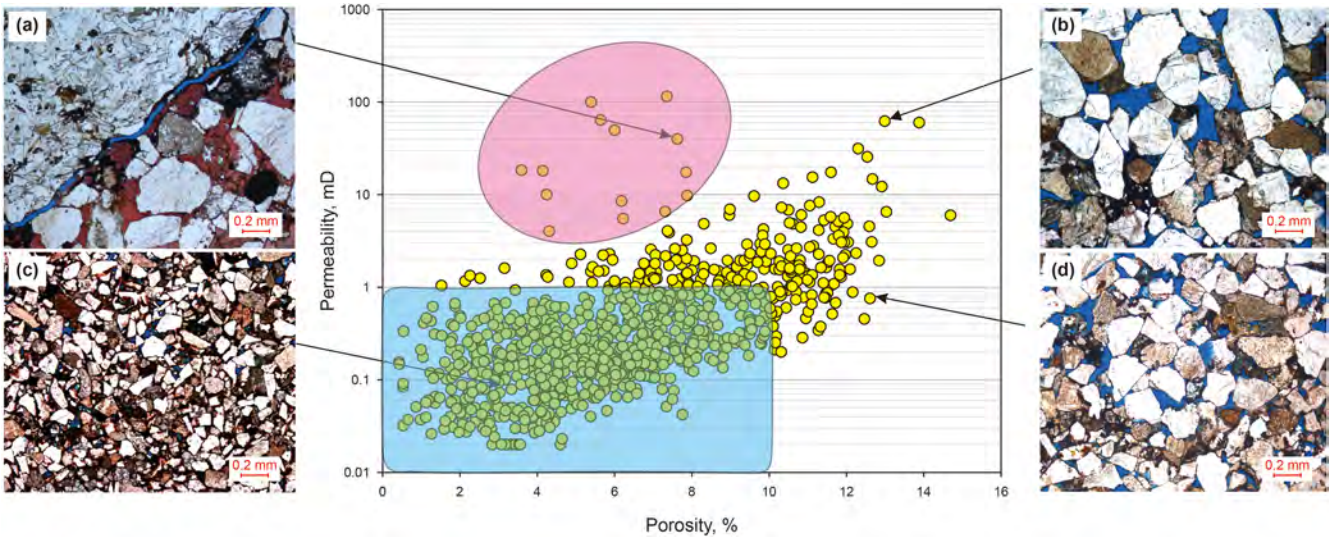

Fig. 3. Relationship between core-measured porosity and permeability for the Cretaceous Bashijiqike Formation in the Kuqa Depression. Thin sections display four types of pore-throat connectivity: **(a)** Low porosity matrix with high permeability due to the presence of microfractures; **(b)** high porosity and high permeability with well-connected intergranular pores; **(c)** low porosity and low permeability due to compaction and cementation; **(d)** high porosity but low permeability due to poorly connected pore throats.

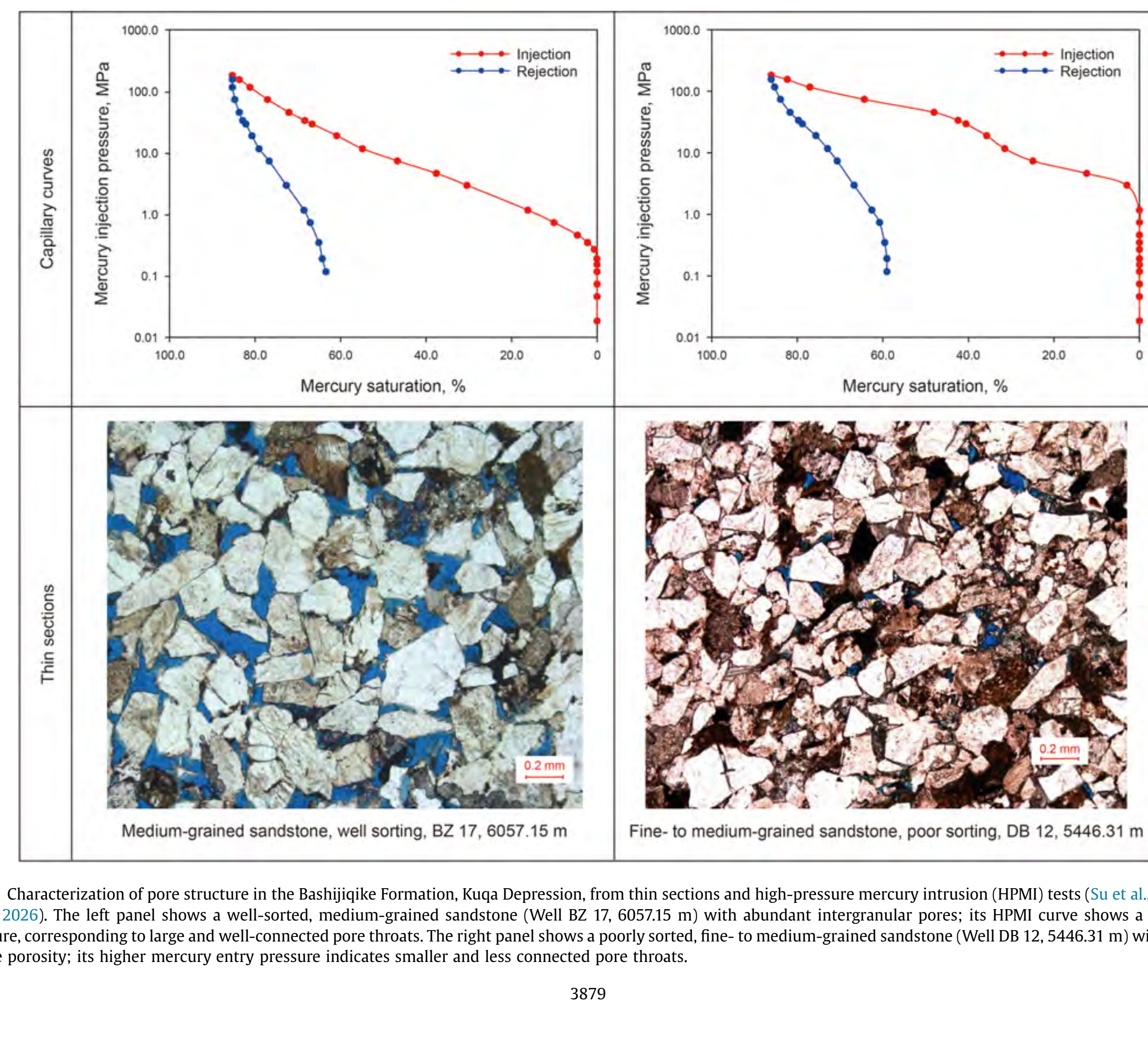

Fig. 4. Characterization of pore structure in the Bashijiqike Formation, Kuqa Depression, from thin sections and high-pressure mercury intrusion (HPMI) tests (Su et al., 2024; Lai et al., 2026). The left panel shows a well-sorted, medium-grained sandstone (Well BZ 17, 6057.15 m) with abundant intergranular pores; its HPMI curve shows a low entry pressure, corresponding to large and well-connected pore throats. The right panel shows a poorly sorted, fine- to medium-grained sandstone (Well DB 12, 5446.31 m) with limited visible porosity; its higher mercury entry pressure indicates smaller and less connected pore throats.

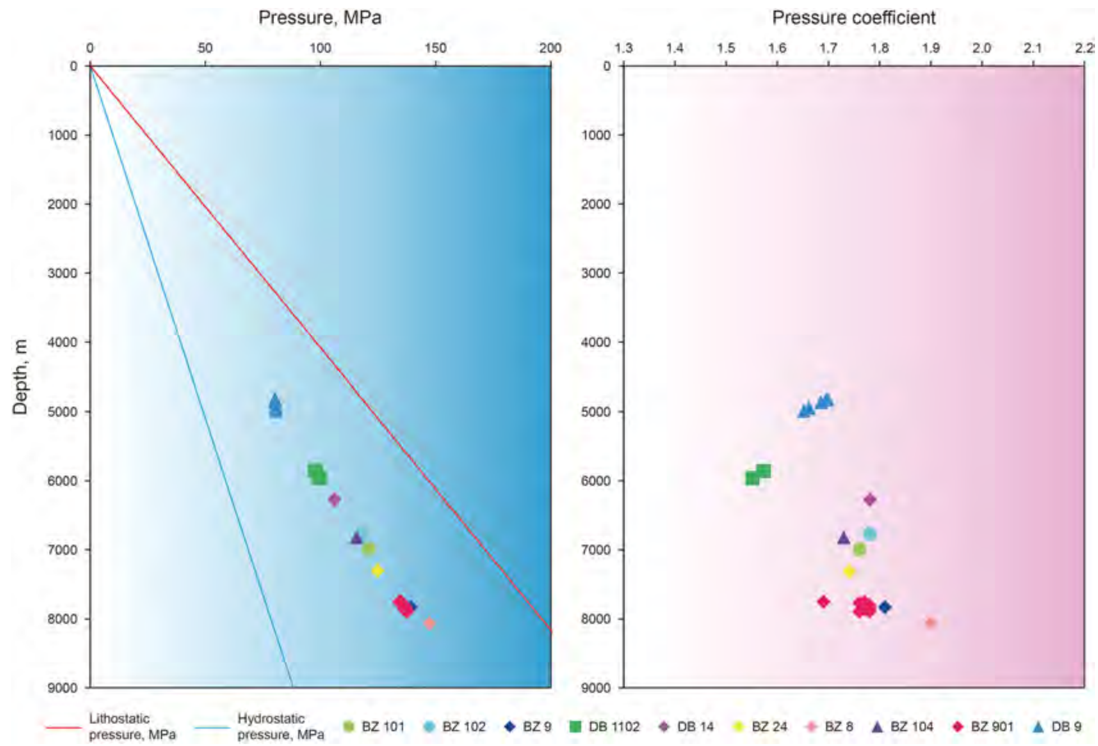

Fig. 5. Pore pressure and pressure coefficient profiles of the Cretaceous Bashijiqike Formation in the Kuqa Depression, from Modular Formation Dynamics Tester (MDT) measurements. The plots show pore pressure (left) and pore pressure coefficient (PPC, right) versus true vertical depth. The data, collected from 10 wells, reveal a strong overpressure regime, with pore pressures reaching 147.32 MPa at 8072.79 m and pressure coefficients as high as 2.1.

were prepared. Triaxial rock mechanics experiments utilized TAW-2000 servo-controlled systems to simulate in-situ stress conditions on standardized plug samples. Coupled X-ray micro-CT imaging (ZEISS Xradia 510 Versa) enables 3D visualization of stress-induced microfracture propagation under true triaxial loading. For the coupled triaxial-CT experiment detailed in Section 4.3, two representative fine- to medium-grained sandstone samples were selected.

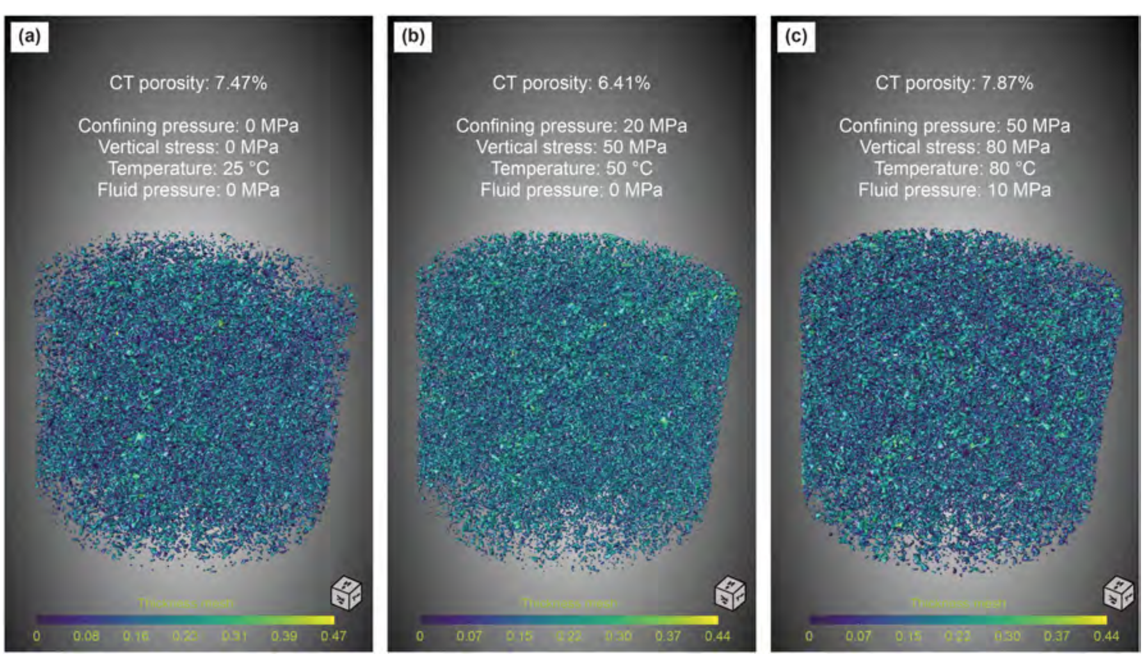

Fig. 6. Experimental results from coupled X-ray micro-CT imaging demonstrating the competing effects of confining pressure, temperature, and pore fluid pressure on sandstone porosity (Wei et al., 2026). **(a)** The initial sample at ambient conditions shows a CT-measured porosity of 7.47%; **(b)** increasing confining pressure (to 50 MPa) and temperature (to 80 °C) without fluid pressure causes a significant porosity decrease, reducing porosity to 6.41%; **(c)** when high pore fluid pressure (10 MPa) is applied along with high confining stress, it counteracts the compactional forces, and the porosity is preserved at 7.87%, nearly its original value.

4. Results

4.1. Reservoir properties

A total of 1026 sets of core analysis were conducted on samples from 18 wells in the Bozi-Dabei Gas Field of Kuqa Depression. Core analysis reveals that the permeability of the sandstones ranges from 0.02 mD to 115 mD. These rocks in the Bozi-Dabei Gas Field, characterized by ultra-low permeability and porosity, consist of complex pore spaces comprising intergranular pores, dissolution pores, and microfractures (Fig. 3). Notably, a significant proportion (79.7%) of the samples exhibit porosity values below 10%, with corresponding air permeability values not exceeding 1 mD (Fig. 3).

Despite the low porosity, some samples exhibit high permeability, which can be attributed to the presence of microfractures (Fig. 3(a)). These microfractures, along with favorable pore throat connectivity, enhance fluid flow even in rocks with low porosity. Samples exhibiting favorable pore throat connectivity and the presence of intragranular micro-fractures exhibit high porosity and high permeability (Fig. 3(b)). In deep and ultra-deep rocks, which have undergone significant compaction and cementation, most samples exhibit both low porosity and low permeability (Fig. 3(c)). Conversely, some other samples show higher porosity but lower permeability, primarily due to poor pore throat connectivity (Fig. 3(d)). The presence of abundant primary intergranular pores suggests that compaction plays a dominant role in diagenetic alterations within these rocks.

Grain size and sorting are crucial in determining the pore systems and pore structure of sandstones. Intergranular pore spaces are always associated with the rocks that are well-sorted and have a coarser grain size, conversely, pores in very fine-grained or poorly-sorted rocks are rare (Fig. 4). In addition, well-sorted and coarse-grained samples have larger pore-throat radii, as evidenced by the HPMI curves (Fig. 4). The fine-grained or poorly-sorted rocks tend to have a high threshold pressure as shown by the HPMI curves (Fig. 4).

4.2. In-situ pore pressure regime

A total of 32 MDT test data from 10 wells enable the precise characterization of pore pressure distribution. In the Cretaceous Bashijiqike Formation of the Bozi-Dabei Gas Field in Kuqa Depression, pore pressures range from 80.21 MPa (4826.39 m) to 147.32 MPa (8072.79 m), with an average pore pressure of 120.65 MPa (Fig. 5). The pore pressure coefficient (PPC), defined as the ratio of measured pore pressure to hydrostatic pressure at equivalent depth, serves as a key indicator for pressure regime characterization. In the Bashijiqike sandstones, the maximum pressure coefficient recorded can reach up to 2.1, indicating the presence of overpressure in the Bozi-Dabei Gas Field in Kuqa Depression (Fig. 5).

4.3. Porosity evolution under triaxial stress and pore pressure

To demonstrate the role of pore pressure in counteracting the effects of confining stress, a set of triaxial tests coupled with CT imaging was conducted on two representative sandstone samples (Wei et al., 2026).

The initial, unstressed state of the sample at ambient conditions (25 °C, 0 MPa confining pressure) exhibited a CT porosity of 7.47% (Fig. 6(a)). In the second stage, conditions were adjusted to simulate burial and compaction. The confining pressure was increased to 20 MPa, vertical stress to 50 MPa, and temperature to 50 °C, while fluid pressure remained at 0 MPa. Under this net compressive stress, the CT porosity decreased to 6.41%, representing an initial porosity reduction of 1.06% (Fig. 6(b)). The final and most critical stage of the experiment demonstrates the counteracting effect of pore pressure (Wei et al., 2026). While the confining stress (50 MPa), vertical stress (80 MPa), and temperature (80 °C) were further increased, a high fluid pressure (10 MPa) was introduced into the pore network, which reduced the effective stress on the rock matrix. Consequently, the CT porosity was recovered to 7.87% by an additional 0.40% relative to the initial porosity value (7.47%) (Fig. 6(c)). This result unequivocally shows that elevated fluid pressure can offset the porosity-reducing effects of mechanical compaction, effectively support the rock frame, and preserve, or even slightly enhance the pore volume (Wei et al., 2026). This principle was consistently observed in the two samples tested, where higher fluid pressure invariably led to an increase in rock porosity (Wei et al., 2026).

4.4. Pore pressure prediction from well logs

The MDT data offer a direct, non-destructive method for evaluating pore pressure, providing real-time, cost-effective insights into the pore pressure (Zhang, 2011; Asfha et al., 2024; Lai et al., 2024). Several empirical approaches for determining pore pressure from well log data include the equivalent depth method, Bowers' method, and Eaton's method, among others (Zhang, 2011; Azadpour et al., 2015). These approaches are grounded in the effective stress theory as originally proposed by Terzaghi (1923) and Biot (1941) (Asfha et al., 2024). Eaton's method predominantly relies on the sonic log velocity trend to construct a baseline normal trend line (Eaton, 1969; Zhang, 2011). For points with abnormal formation pressure, the sonic transit time will deviate from the normal trend line, and the degree of deviation is related to the magnitude of the pore pressure anomaly. Utilizing Eaton's method to calculate the pore pressure, the basic form of the pressure estimation formula is expressed as follows (Eq. (2)):

$$P_{\mathrm{p}} = P_0 - (P_0 - P_{\mathrm{w}})\left(\frac{\Delta t_{\mathrm{n}}}{\Delta t}\right)^c \tag{2}$$

where P_{p} is the formation pressure; P_0 is the overburden pressure; P_{w} is the hydrostatic pore pressure; Δt is the measured sonic transit time in shale by well logging; Δt_{n} is the sonic transit time in shale at the normal pressure condition obtained from normal trend line; c is the exponent constant.

Crossplot analysis reveals that the calculated pore pressures have a strong linear correlation ($R^2 = 0.9641$) with the measured pore pressures in the Bashijiqike Formation of Kuqa Depression

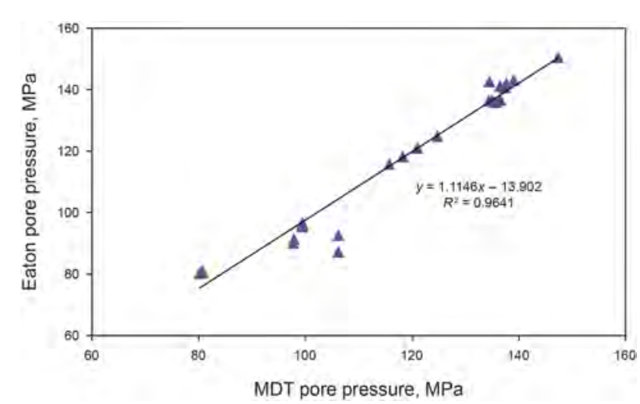

Fig. 7. The crossplot of pore pressure measured by MDT versus pore pressure calculated by Eaton's method of the Bashijiqike Formation in Kuqa Depression.

(Fig. 7). This indicates that Eaton's method has high accuracy in predicting pore pressure.

4.5. Well log evaluation of fracture

Fracture characteristics, including dip, strike, azimuth, and aperture, can be interpreted from borehole image logs (Fernández-Ibáñez et al., 2018). The integration of conventional well logs, image logs, and cores facilitates the identification of fractures in deep and ultra-deep rocks.

In fracture zones, the bulk density log (RHOB) exhibits marked reductions due to fluid invasion into fractures. Compressional (P wave) and shear (S wave) amplitudes attenuate, while Stoneley wave energy dissipation intensifies. Interval transit time (Δt) exhibits notable increases in fractured intervals. On electronic borehole images, fractures manifest as clear lines that vary in appearance based on their angle in relation to the path of the borehole. Notably, fractures exhibit continuous or discontinuous conductive, resistive, or mixed sinusoidal patterns in borehole images (Lai et al., 2017; Fernández-Ibáñez et al., 2018; Su et al., 2026).

Observing the cores, seven fractures can be extracted (Fig. 8). Meanwhile, seven corresponding fractures were identified in the image logs at the same depth interval (6057.0–6059.0 m) (Fig. 8).

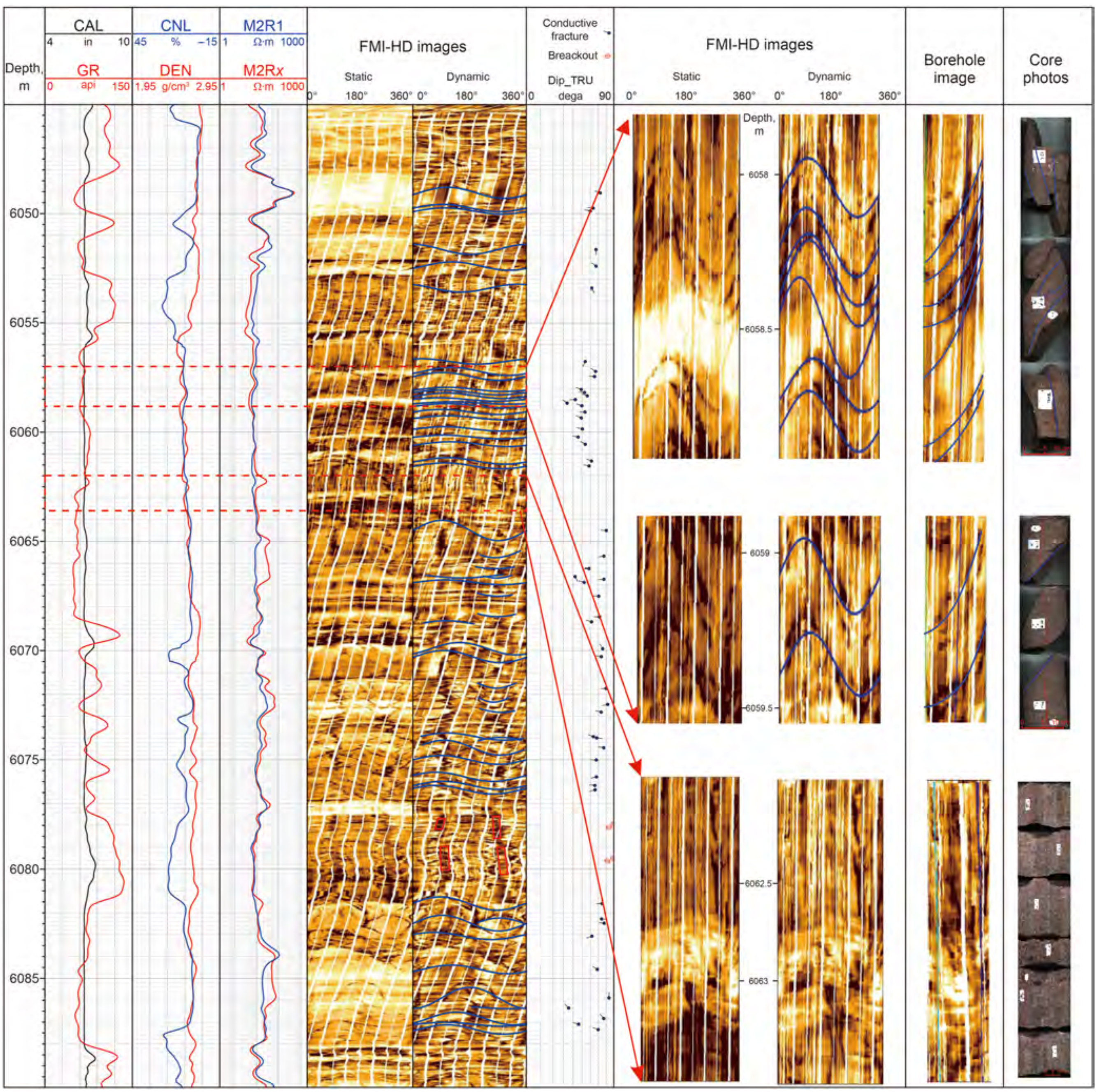

Fig. 8. Integrated fracture identification using conventional well logs, high-resolution borehole image logs, and drilled cores from Well BZ 17. The FMI-HD images display fractures as conductive (dark) sinusoidal features. Direct comparison with core photos from the same depth intervals (6057–6059 m) confirms the presence and orientation of fractures identified in the logs.

Conversely, no fractures were detected in the well interval (6062.0–6063.5 m) in the corresponding image logs and cores (Fig. 8). This demonstrates the capacity of image logs to precisely identify fractures and the consistency between different data sources (including cores and well logs).

4.6. Structural patterns and pore pressure

The increase in pore pressure arises from the buoyancy of hydrocarbons, which is a consequence of the density discrepancy between hydrocarbon and brine (Towler, 2002; Zhang, 2011). As the height of the hydrocarbon column rises, the buoyant force increases, allowing gas to overcome higher capillary pressures and infiltrate through spaces with smaller throat radii. Consequently, gas column height directly influences the pore pressure within the reservoir.

In the DB 9 well block, data reveal a significant correlation between pore pressure and gas column height, as depicted in Fig. 9. The pore pressure and pressure coefficient were calculated using Eaton's method. Within a continuous hydrocarbon column, pore pressure increases with structural elevation above the gas-water contact in the DB 9 well block (Fig. 9). These findings align with our expectations, confirming that the pore pressure within the trap is governed by the gas column height above the gas-water interface. As the distance from the gas-water contact increases, the gas column height increases, consequently leading to an increase in pore pressure.

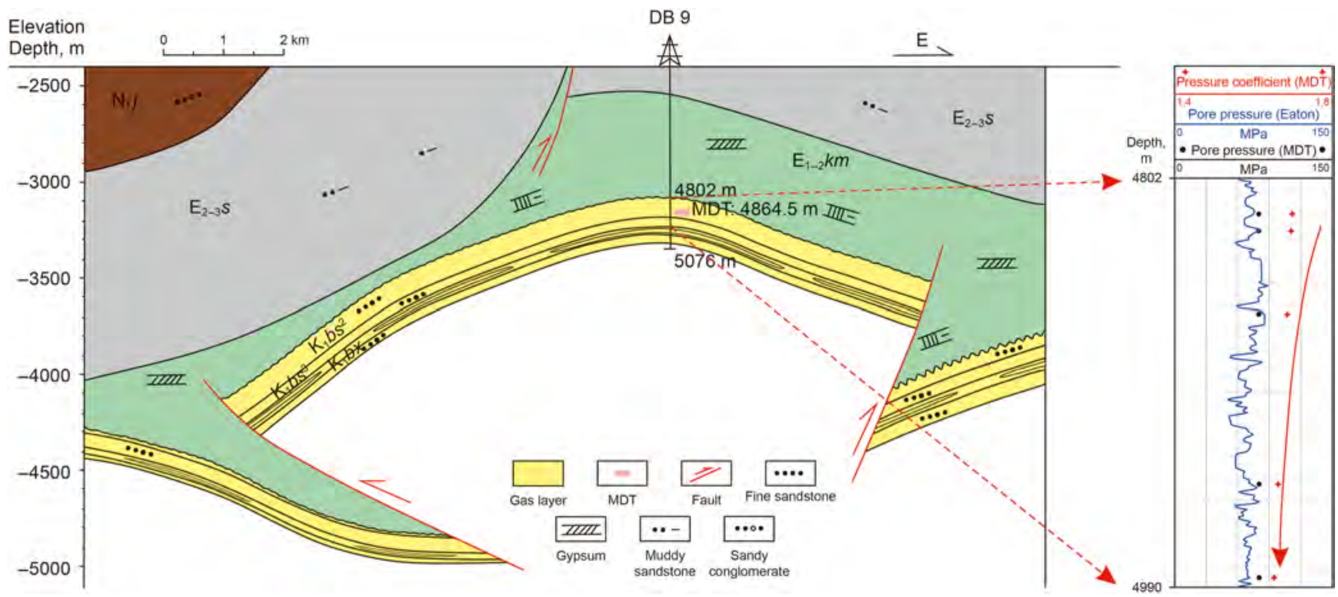

Fig. 9. Relationship between pore pressure (pressure coefficient) and burial depth of Bashijiqike Formation in the DB 9 well block in Kuqa Depression. The plot shows that as the gas column height increases, both pore pressure and the pressure coefficient rise accordingly, confirming that hydrocarbon buoyancy is the dominant control on pore pressure within the trap.

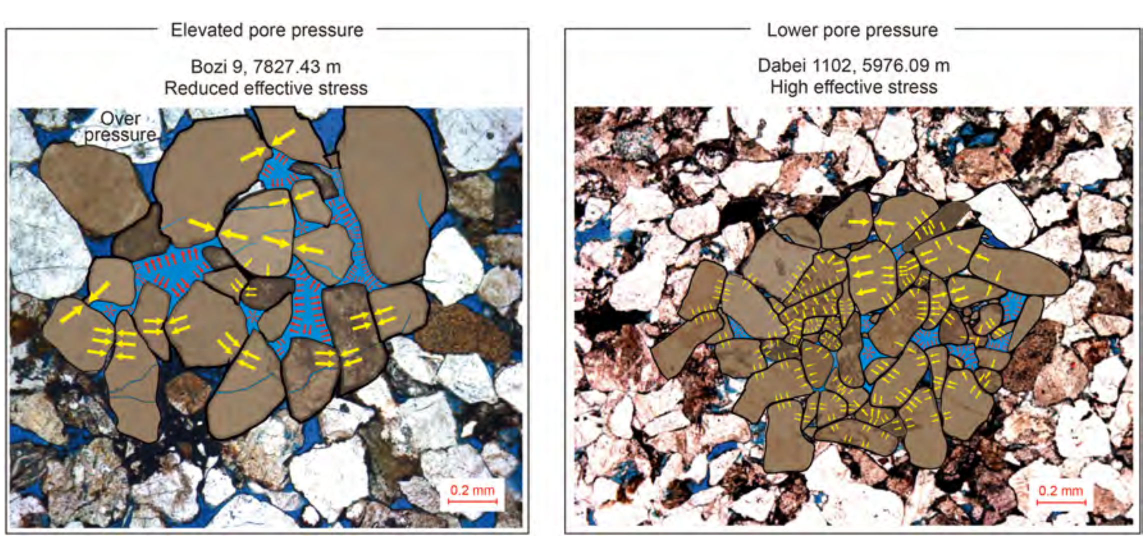

Fig. 10. A conceptual model showing porosity preservation with pore pressure for elevated pore pressure (left) and lower pore pressure (right) respectively in the Kuqa Depression. Left: strongly overpressured Well BZ 9 (7827.43 m), pore pressure about 1.88 and abundant primary intergranular porosity. Right: medium pore pressure with pore pressure about 1.55 in Well DB 1102 (5976.09 m), showing intense mechanical compaction, and concavo-convex to sutured contacts. Red arrows indicate porosity preservation due to reduced effective stress under overpressure; yellow arrows indicate mechanical compaction between grains.

5. Discussion

5.1. Pore pressure and porosity preservation

5.1.1. Schematic model for porosity preservation by overpressure

When sediment permeability is insufficient to permit effective expulsion of pore fluids, overpressures develop as retained fluids bear a portion of the overburden stress (Hart et al., 1995). The elevated pore pressure often contributes to higher porosity in rocks under higher pressure compared to their counterparts at the same depth with normal pressure (Hart et al., 1995; Screaton et al., 2002; Siggins and Dewhurst, 2003; Spinelli et al., 2007; Nikolinakou et al., 2023).

Microstructural observations from wells with contrasting pressure regimes provide evidence of this mechanism. A conceptual model based on thin sections illustrates this process clearly (Fig. 10). In Well BZ 9 with strong overpressure (pore pressure coefficient 1.88), primary intergranular porosity remains well-preserved, with grain contacts that are predominantly point-to-line, even at depths exceeding 7800 m (Fig. 10). Additionally, microfractures are observed in the thin sections from this well (Fig. 10).

Conversely, in reservoirs with lower pore pressure (pore pressure coefficient 1.55), such as those encountered in the Well DB 1102 (Fig. 10), the framework grains bear the majority of the lithostatic load, resulting in high effective stress. The microscopic thin sections from this well demonstrate the predictable outcome: severe mechanical compaction has led to a dense grain packing, characterized by concavo-convex and sutured grain contacts and rare primary pores, and the near-total occlusion of primary porosity (Fig. 10).

5.1.2. Quantitative relationship between porosity and pore pressure

As revealed in the porosity evolution history and pore pressure evolution history of Fig. 2 (Guo et al., 2016c; Zeng et al., 2020),

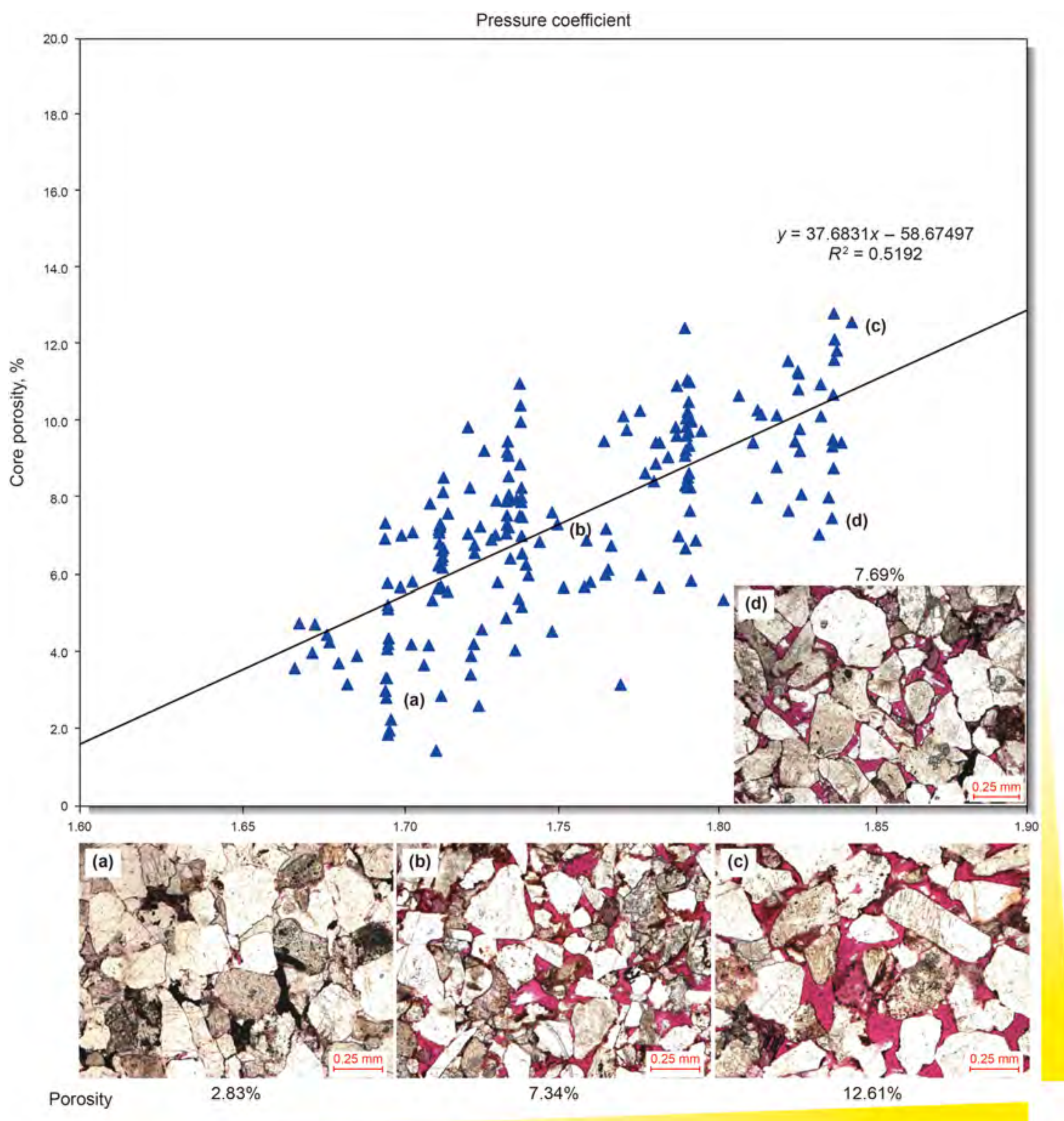

Fig. 11. The positive correlation between pore pressure coefficient and core-measured porosity. Thin sections (red epoxy impregnates pores) provide micro-scale evidence of this process: **(a)** low porosity (2.83%) with sutured grain contacts under near-normal pressure conditions (pressure coefficient ≈ 1.65); **(b)** moderate porosity (7.34%) with more prevalent line contacts is observed at a lower pressure coefficient (≈1.75); **(c)** high porosity (12.61%) and point-line grain contacts are preserved under high overpressure (pressure coefficient ≈ 1.85); **(d)** a poorly sorted sandstone exhibits lower porosity (7.69%) than (c) despite being in an overpressured environment.

overpressure occurs at approximately 5 Ma, and the porosity reduction rate is low even when rapidly and deeply buried to as deep as 8000 m (Fig. 2(c)). Therefore the process of porosity preservation was initiated at the time of overpressure generation (Fig. 2(b) and (c)) (Guo et al., 2016c).

Additionally, a crossplot of pressure coefficient versus core porosity is constructed, revealing a positive correlation between these two parameters in the fine- to medium-grained sandstones, with higher pressure coefficient corresponding to increased porosity (Fig. 11). Porosity can be maintained as high as 6% even at

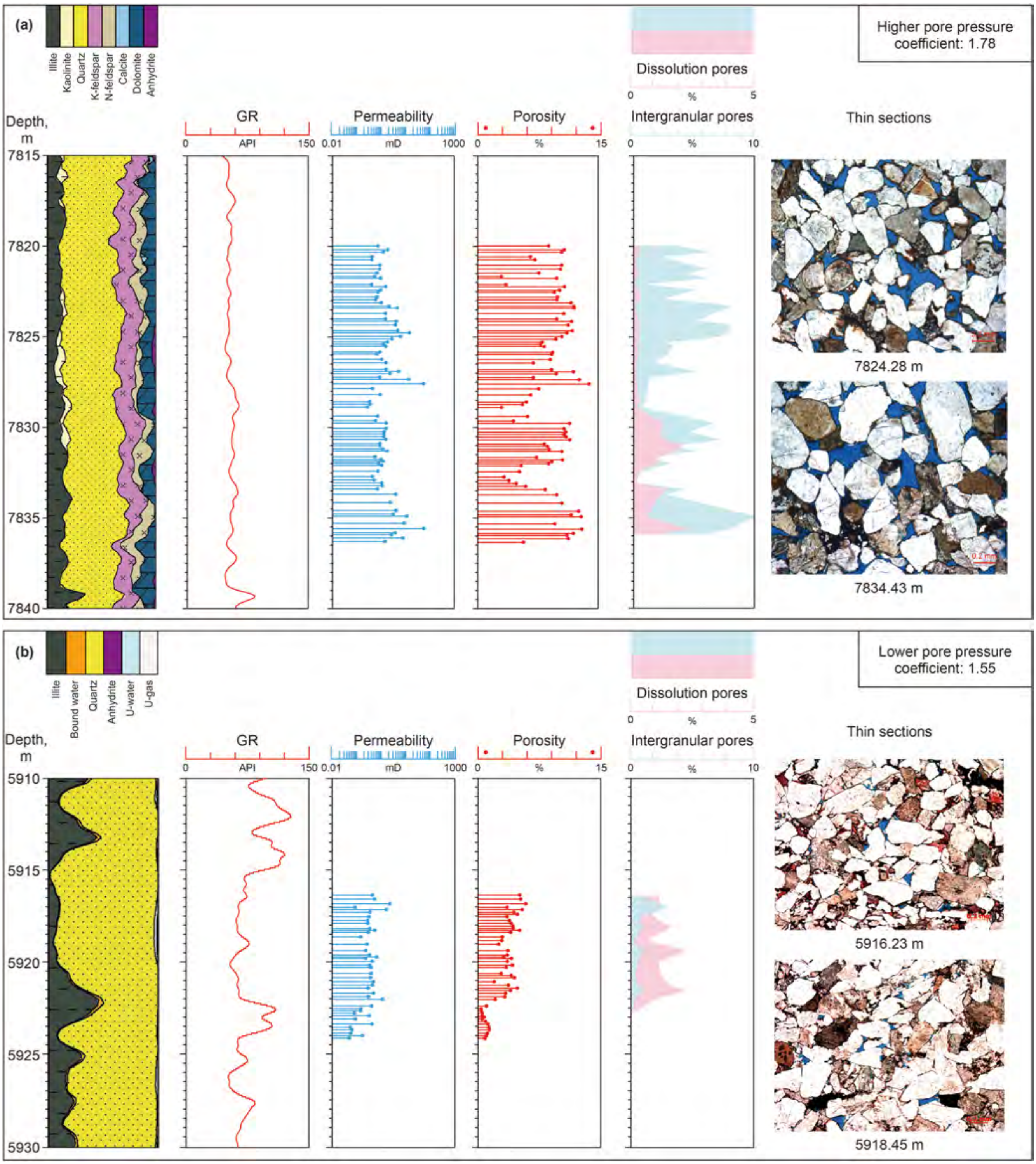

Fig. 12. Single-well column graphs demonstrating the direct influence of pore pressure on petrophysical properties and pore systems in the Cretaceous Bashijiqike Formation in Kuqa Depression. Pore pressure control on reservoir properties in the Bashijiqike Formation: **(a)** Well BZ 901: high pore pressure (1.78) limits compaction, preserving primary porosity and high permeability; **(b)** Well DB 1102: lower pore pressure (1.55) causes intense compaction, degrading the reservoir. GR (API), permeability (mD), porosity (%), and pore type distributions are shown alongside representative thin sections (blue epoxy impregnating pores).

depths exceeding 6000 m when the pressure coefficient is higher than 1.75 (Fig. 11). However, there are some data points with low porosity even at high pressure conditions, therefore the elevated pore pressure is not the sole controlling factor for inhibiting compaction and porosity preservation. Composition and texture of sandstones also control the porosity preservation processes, and preservation of porosity values exceeding 6.0% is mainly associated with the well-sorted and medium-grained sandstones (Fig. 11(b) and (c)). Very fine-grained or poorly sorted sandstones have no ability for porosity preservation even at high pore pressure conditions (Fig. 11(d)).

As revealed in the thin sections of Fig. 11, in the fine- to medium-grained and well-sorted sandstones, the increasing pressure coefficient contributes to a preservation of intergranular pore spaces, as evidenced by the grain contacts changing from line contact to point-line contact (Fig. 11(a) and (b)). The intergranular pores are commonly preserved in the well-sorted and fine- to medium-grained sandstones, whereas poorly-sorted sandstones are easily tightly compacted even under overpressure environments (Fig. 11(c) and (d)). This demonstrates that the effectiveness of overpressure in porosity preservation is highly dependent on the host rock's textural maturity.

5.2. Relationships between porosity and overpressure in single wells

Two single wells are used to unravel the relationships between porosity and overpressure. In the Well BZ 901, pore pressure coefficient in the interval 7815–7840 m reaches 1.78 (Fig. 12(a)). The elevated pressure effectively counteracts the overburden stress, leading to a good preservation of porosity at a depth of approximately 7820 m (Fig. 12(a)). The LithoScanner well log data show the lithology is medium-grained sandstone, and the core-measured porosity ranges from 10% to 15% and permeability frequently exceeds 100 mD (Fig. 12(a)). Thin sections show that the pore types in these intervals are dominated by primary intergranular pores, which suggests that overpressure has inhibited mechanical compaction.

In Well DB 1102, pore pressure coefficient in the intervals 5910–5930 m is 1.55. Despite being at a shallower depth (5920 m) (Fig. 12(b)), core-measured porosity is lower and significantly more heterogeneous, generally below 10%, while permeability is drastically reduced to values typically less than 10 mD (Fig. 12(b)). The decrease in porosity and permeability is attributed to intense mechanical compaction, which reduced the intergranular pore volume. This conclusion is supported by thin section analysis, which shows a low content of intergranular pores (Fig. 12(b)).

5.3. Pore pressure and fracture aperture

Natural fractures in low-permeability rocks serve as critical fluid pathways, with their mechanical behavior highly sensitive to pore pressure variations. Elevated pore pressure reduces effective stress, promoting the openness of fractures (Baghbanan and Jing, 2008; Becker et al., 2010; Wang et al., 2020a; Cao et al., 2021). Elevated pore pressures induce leftward migration of the Mohr stress circle (Zeng et al., 2023). At critical failure envelope conditions, the effective minimum principal stress transitions from compressive to tensile regimes, facilitating the development of overpressure-induced fractures (Zeng et al., 2023). Meanwhile, pore pressure can facilitate the openness of early-formed fractures.

To precisely quantify the relationship between overpressure and fractures, wells drilled with water-based muds were selected for analysis. This study focuses on the mechanical aperture, which represents the physical opening of the fracture as measured by borehole imaging tools, rather than the hydraulic aperture. The correlations between pore pressures measured by MDT and mechanical fracture apertures at the same depth are quantified. The result indicates a strong positive relationship between the pressure coefficient (MDT) and mechanical fracture aperture (Fig. 13). As can be observed in the image logs, fractures are commonly detected in the fine to medium grained sandstones (Fig. 13). Notably, the mechanical aperture can reach values as high as 4.7 mm where the pore pressure coefficient is higher than 1.75 in these fine- to medium-grained sandstones (Fig. 13). Well BZ 104 exhibits a higher fracture aperture at elevated pressure coefficient compared to Well DB 1102, which shows reduced fracture apertures at lower pressure coefficient. As the pressure coefficient increases, the fracture aperture also tends to increase in the fine- to medium-grained sandstones (Fig. 13).

5.4. Pore pressure effects on microscopic pore structure

The pore pressure controls the microscopic pore structure. Fig. 14 reveals that the pressure coefficient exhibits a positive correlation with maximum connected pore radius (Fig. 14(a)), while the horizontal stress difference ($S_{\mathrm{hmax}} - S_{\mathrm{hmin}}$) demonstrates a negative correlation with maximum connected pore radius (Fig. 14(b)). High pore pressure, which reduces the effective stress

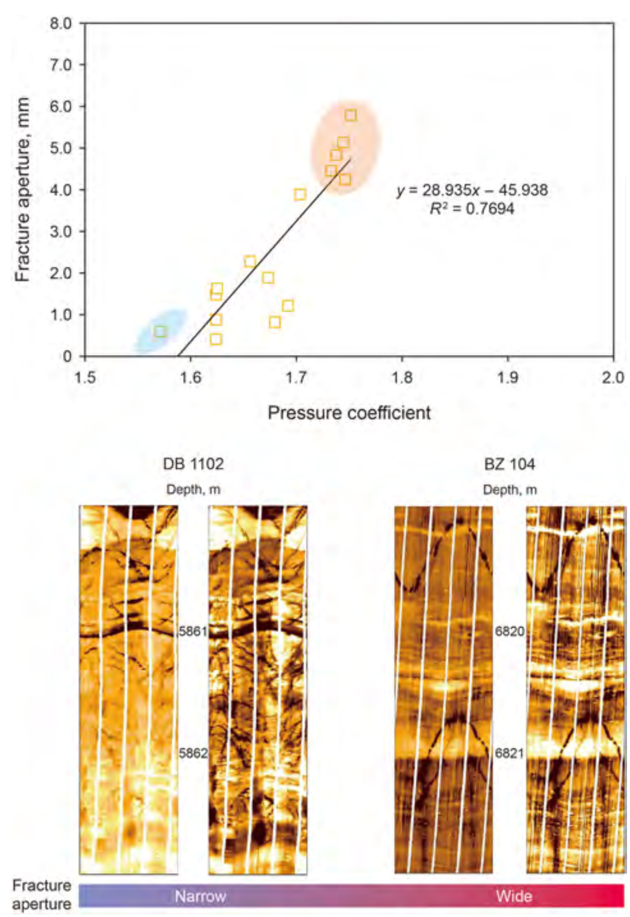

Fig. 13. Quantitative analysis of the relationship between pore pressure coefficient (from MDT) and mechanical fracture aperture (from image logs). The crossplot reveals a strong positive correlation ($R^2 = 0.7694$), indicating that higher overpressure promotes the opening of natural fractures.

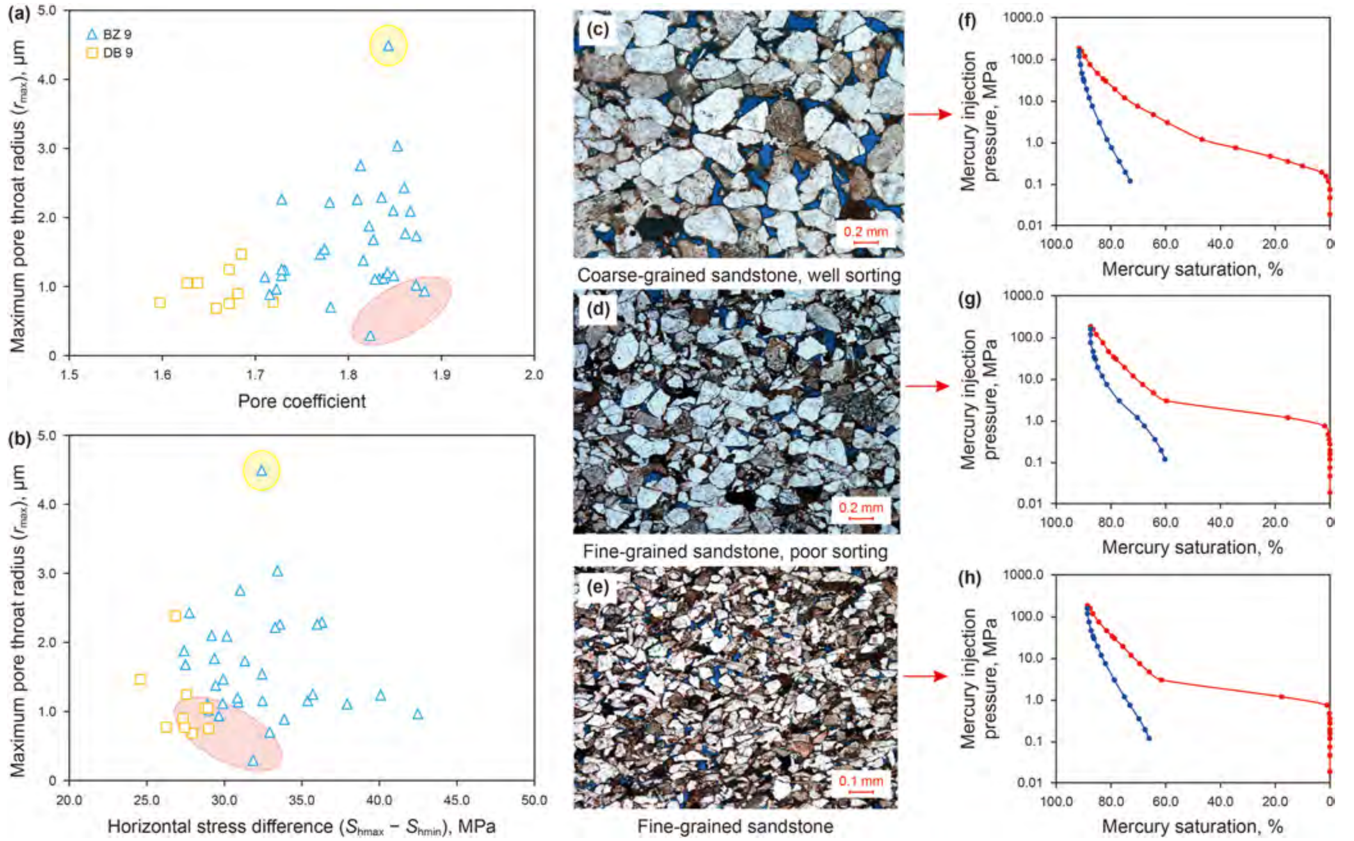

Fig. 14. Analysis of the relationship between in situ stress (pore pressure and horizontal stress difference) and maximum pore throat radius in the Kuqa Depression using thin sections and HPMI tests: **(a)** r_{max} shows a positive correlation with the pore pressure coefficient, suggesting overpressure helps keep pore throats open; **(b)** r_{max} exhibits a negative correlation with the horizontal stress difference; **(c)–(h)** Thin sections and corresponding HPMI curves show that this effect is most pronounced in coarse-grained, well-sorted sandstones (c), while in poorly sorted or fine-grained sandstones ((d) and (e)), pore throats remain small regardless of the pressure regime.

on the rock's grain framework (Hart et al., 1995; Osborne and Swarbrick, 1997), inhibits mechanical compaction and pressure dissolution. This process is critical for preserving the primary pore network and helps to keep pore throats open, especially when overpressure develops early in the burial history (Screaton et al., 2002; Stricker and Jones, 2018; Nikolinakou et al., 2023). There are some exceptions, and high pore pressure is not always associated with high porosity and wide pore throat radius. For the poorly sorted or very fine-grained rocks, high pore pressure has less potential to keep the pore throat open (Fig. 14(c)). Actually, poorly sorted or very fine-grained rocks will experience a high degree of compaction during deep burial (Ozkan et al., 2011; Bjørlykke and Jahren, 2012; Lai et al., 2018).

5.5. Model of pore pressure effect on reservoir properties

Integrating the previous findings, a geological model is constructed to characterize a fold-and-thrust belt and quantitatively assess how the pore pressure variation controls reservoir properties (Obradors-Prats et al., 2017). By synthesizing pore structure and fracture characteristics with calculated pore pressure (calibrated by MDT), the interplay between pore pressure distribution and reservoir properties is elucidated.

In the BZ 1 well block, Eaton's method is used to calculate the pore pressure. The wells BZ 101 and BZ 104 have relatively higher pore pressure, while the Well BZ 102, located at a higher stratigraphic position, has relatively lower pore pressure (Fig. 15). The data reveals that the fold-and-thrust belt likely created pressure compartments, with the fore-thrust and back-thrust (wells BZ 101 and BZ 104) retaining overpressure due to fault seal integrity (Fig. 15(e), (g)). However, the location near the axial plane of the anticline (BZ 102) experiences pressure dissipation (Fig. 15(f)). Notably, the pressure-sealed compartments in the fore-thrust (BZ 101) and back-thrust (BZ 104) have higher pore pressure and better reservoir properties compared to compartments in the lifted wedge (BZ 102) (Fig. 15(c), (d), (e), (g)).

Meanwhile, the sandstones with higher pore pressure (BZ 101 and BZ 104) (Fig. 15(e), (g)) preserve higher porosity than their counterparts with normal pressure (BZ 102) (Fig. 15(f)) (Wang et al., 2023). The observed higher porosity in the reservoirs with higher pore pressure (BZ 101 and BZ 104) supports the "pressure-dependent porosity preservation" hypothesis (Hart et al., 1995; Osborne and Swarbrick, 1997; Screaton et al., 2002; Siggins and Dewhurst, 2003; Spinelli et al., 2007; Nikolinakou et al., 2023). By resisting effective stress, overpressure reduces grain-to-grain contact forces, thereby inhibiting mechanical compaction during burial (Siggins and Dewhurst, 2003; Spinelli et al., 2007; Nikolinakou et al., 2023) (Fig. 15). This phenomenon is particularly pronounced in quartz-rich sandstones (Bjørlykke, 2014).

The BZ 1 block (including wells BZ 101, BZ 102, and BZ 104) exhibits a strike-slip fault regime, with the stress magnitudes arranged as S_{hmax} (maximum horizontal stress) > S_v (vertical stress) > S_{hmin} (minimum horizontal stress) (Zoback, 1992; Townend and Zoback, 2000). The differential stress parameter ($S_{hmax} - P_p$) is used to evaluate the impact of the stress field on the later-stage modification of fractures. Analytical results further reveal pore pressure's dual role: an increase in pore pressure (P_p) reduces the effective stress, which in turn promotes openness of

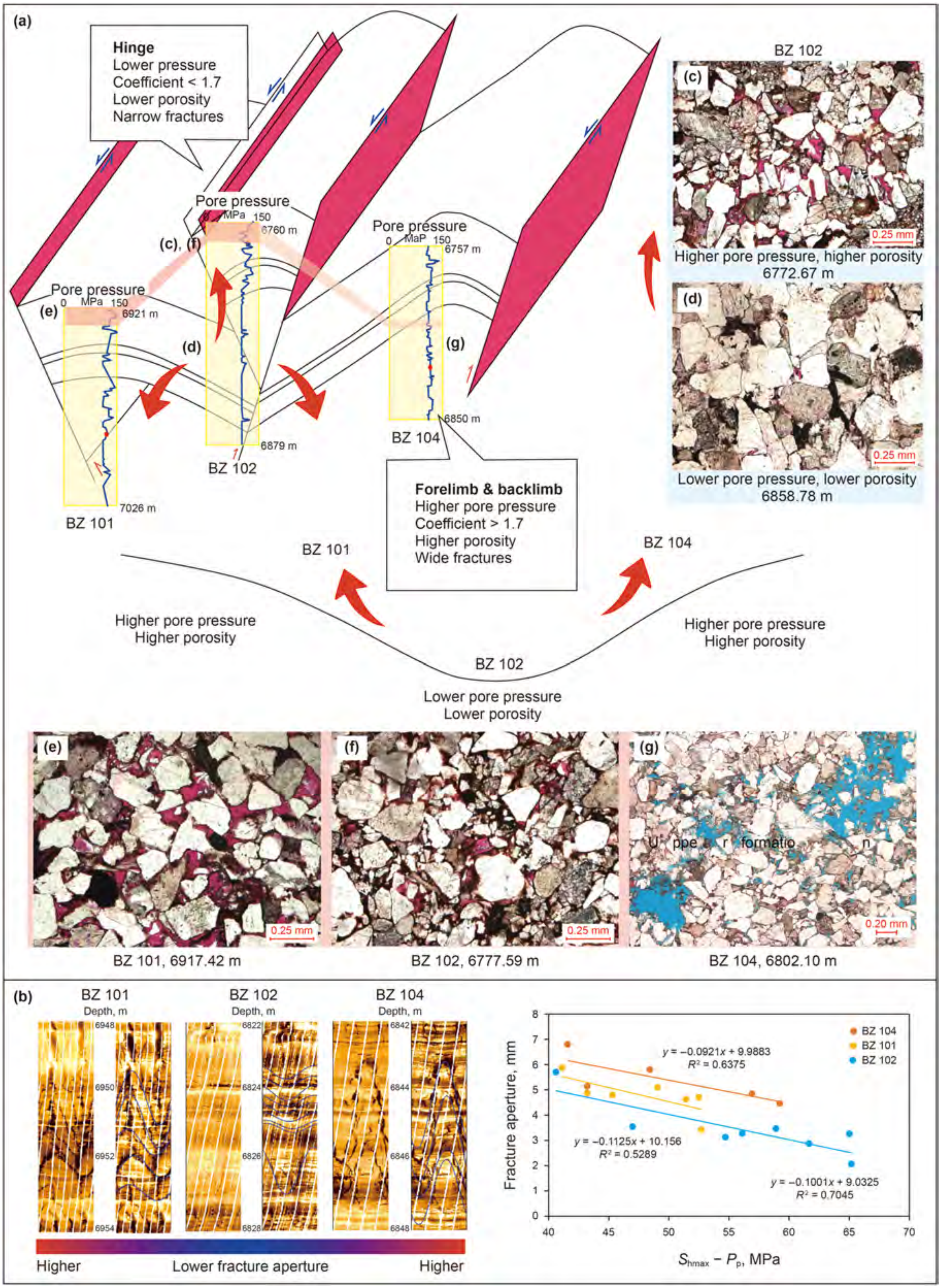

Fig. 15. Integrated schematic model illustrating the effect of pore pressure on multi-scale reservoir properties across different structural positions in the BZ 1 fold-and-thrust block. **(a)** Cross-section reveals higher pore pressure in the structurally fore-thrust zone (BZ 101) and back-thrust zone (BZ 104) compared to the lifted wedge (BZ 102); **(b)** demonstrates that fracture aperture is wider in the high-pressure wells, a relationship quantified by the negative correlation between aperture and the effective stress parameter.

pre-existing fractures (Fig. 15) (Gudmundsson, 2011). When pore pressure is high, the fracture aperture tends to be wider (Baghbanan and Jing, 2008; Cao et al., 2021). As shown in Fig. 15(b), the fracture aperture in Well BZ 102 is narrower compared to that in wells BZ 101 and BZ 104, which further validates the previously stated conclusion.

Overall, reservoir properties are dynamically shaped by tectonically driven pore pressure evolution. Meanwhile, the oil tests of three wells show that the daily natural gas production of wells BZ 101 (Fig. 15(e)) and BZ 104 (Fig. 15(g)) is higher than that of Well BZ 102 (Fig. 15(f)). The fore-thrust and back-thrust emerge as sweet spots where overpressure synergistically preserves porosity and promotes fracture opening, offering a conceptual model for analogous fold-and-thrust belts (Obradors-Prats et al., 2017).

6. Conclusions

This study provides a quantitative framework for understanding the multi-scale effects of pore pressure on reservoir properties in deep and ultra-deep sandstones.

1) Elevated pore pressure mechanically inhibits compaction-driven porosity loss, and a pore pressure coefficient exceeding 1.75 maintains matrix porosity up to 6.0% at 7000 m or deeper.
2) High pore pressure promotes the openness of natural fractures. A positive correlation exists between the pore pressure coefficient and fracture aperture, with apertures reaching 4.7 mm where the coefficient exceeds 1.75.
3) Pore pressure positively influences microscopic pore structure. In coarse-grained and well-sorted sandstones, a pore pressure coefficient above 1.75 corresponds to a maximum connected pore throat radius ($r_{\max}$) greater than 1.0 μm.
4) In fold-and-thrust belts, structural position governs pore pressure distribution and reservoir properties. Overpressured fore-thrust and back-thrust structural positions represent optimal targets, characterized by higher pore pressure due to superior porosity preservation and enhanced fracture openness.

CRediT authorship contribution statement

Yang Su: Writing – review & editing, Writing – original draft, Methodology, Data curation, Conceptualization. **Jin Lai:** Writing – review & editing, Methodology, Funding acquisition, Conceptualization. **Wen-Le Dang:** Investigation, Data curation. **Rong-Hu Zhang:** Data curation. **Kai-Xun Zhang:** Data curation. **Yi Xin:** Data curation. **Xiang Shan:** Data curation. **Gui-Wen Wang:** Writing – review & editing, Writing – original draft, Methodology, Conceptualization.

Data availability

The data that support the findings of this study are available from the authors.

Declaration of interests

The authors declare that they have no known competing financial interests or personal relationships that could have appeared to influence the work reported in this paper.

Acknowledgements

This work is financially supported by National Science and Technology Major Project of China (No. 2025ZD1402106), State Key Laboratory of Petroleum Resources and Engineering (No. PRE/indep-2501) and Science Foundation of China University of Petroleum, Beijing (No. 2462023QNXZ010). We sincerely thank the five anonymous reviewers for their constructive comments, which improve the quality of this study. We also thank the editors of the Petroleum Science for their kind editing works.

References

Anderson, B., Hancock, S., Wilson, S., et al., 2011. Formation pressure testing at the Mount Elbert gas hydrate stratigraphic test well, Alaska North slope: Operational summary, history matching, and interpretations. Mar. Petrol. Geol. 28 (2), 478–492. https://doi.org/10.1016/j.marpetgeo.2010.02.012.

Asfha, D.T., Gebretsadik, H.T., Latiff, A.H.A., et al., 2024. Predictive pore pressure modeling using well-log data in the West Baram Delta, offshore Sarawak Basin, Malaysia. Geomech. Geophys. Geo Energy Geo Resour. 10 (1), 196. https://doi.org/10.1007/s40948-024-00903-5.

Azadpour, M., Shad Manaman, N., Kadkhodaie-Ilkhchi, A., et al., 2015. Pore pressure prediction and modeling using well-logging data in one of the gas fields in south of Iran. J. Petrol. Sci. Eng. 128, 15–23. https://doi.org/10.1016/j.petrol.2015.02.022.

Baghbanan, A., Jing, L., 2008. Stress effects on permeability in a fractured rock mass with correlated fracture length and aperture. Int. J. Rock Mech. Min. Sci. 45 (8), 1320–1334. https://doi.org/10.1016/j.ijrmms.2008.01.015.

Barker, C., Takach, N.E., 1992. Prediction of natural gas composition in ultradeep sandstone reservoirs. AAPG Bull. 76 (12), 1859–1873. https://doi.org/10.1306/BDFF8B00-1718-11D7-8645000102C1865D.

Becker, S.P., Eichhubl, P., Laubach, S.E., et al., 2010. A 48 m.y. history of fracture opening, temperature, and fluid pressure: Cretaceous Travis Peak Formation, East Texas basin. Geol. Soc. Am. Bull. 122 (7–8), 1081–1093. https://doi.org/10.1130/B30067.1.

Biot, M.A., 1941. General theory of three-dimensional consolidation. J. Appl. Phys. 12 (2), 155–164. https://doi.org/10.1063/1.1712886.

Bjørlykke, K., 2014. Relationships between depositional environments, burial history and rock properties. Some principal aspects of diagenetic process in sedimentary basins. Sediment. Geol. 301, 1–14. https://doi.org/10.1016/j.sedgeo.2013.12.002.

Bjørlykke, K., Jahren, J., 2012. Open or closed geochemical systems during diagenesis in sedimentary basins: Constraints on mass transfer during diagenesis and the prediction of porosity in sandstone and carbonate reservoirs. AAPG Bull. 96 (12), 2193–2214. https://doi.org/10.1306/04301211139.

Bloch, S., Lander, R.H., Bonnell, L., 2002. Anomalously high porosity and permeability in deeply buried sandstone reservoirs: Origin and predictability. AAPG Bull. 86 (2), 301–328. https://doi.org/10.1306/61EEDABC-173E-11D7-8645000102C1865D.

Cao, H., Nakagawa, S., Askari, R., 2021. Laboratory measurements of the impact of fracture and fluid properties on the propagation of Krauklis waves. J. Geophys. Res. Solid Earth 126 (10), e2020JB021593. https://doi.org/10.1029/2020JB021593.

Dutton, S.P., Loucks, R.G., 2010. Diagenetic controls on evolution of porosity and permeability in lower Tertiary Wilcox sandstones from shallow to ultradeep (200–6700m) burial, Gulf of Mexico Basin, U.S.A. Mar. Petrol. Geol. 27 (1), 69–81. https://doi.org/10.1016/j.marpetgeo.2009.08.008.

Eaton, B.A., 1969. Fracture gradient prediction and its application in oilfield operations. J. Petrol. Technol. 21 (10), 1353–1360. https://doi.org/10.2118/2163-PA.

Fan, C., Wang, G., Wang, Z., et al., 2021. Prediction of multiple origin overpressure in deep fold-thrust belt: A case study of Kuqa subbasin, Tarim Basin, northwestern China. AAPG Bull. 105 (8), 1511–1533. https://doi.org/10.1306/01282119044.

Fernández-Ibáñez, F., DeGraff, J.M., Ibrayev, F., 2018. Integrating borehole image logs with core: A method to enhance subsurface fracture characterization. AAPG Bull. 102 (6), 1067–1090. https://doi.org/10.1306/0726171609317002.

Geng, Y., Liang, W., Liu, J., et al., 2017. Evolution of pore and fracture structure of oil shale under high temperature and high pressure. Energy Fuel. 31 (10), 10404–10413. https://doi.org/10.1021/acs.energyfuels.7b01071.

Gudmundsson, A., 2011. Rock Fractures in Geological Processes. Cambridge University Press, Cambridge. https://doi.org/10.1017/CBO9780511975684.

Guo, X., Liu, K., Jia, C., et al., 2016a. Effects of early petroleum charge and overpressure on reservoir porosity preservation in the giant Kela-2 gas field, Kuqa Depression, Tarim Basin, Northwest China. AAPG Bull. 100 (2), 191–212. https://doi.org/10.1306/11181514223.

Guo, X., Liu, K., Jia, C., et al., 2016b. Fluid evolution in the Dabei Gas Field of the Kuqa Depression, Tarim Basin, NW China: implications for fault-related fluid flow. Mar. Petrol. Geol. 78, 1–16. https://doi.org/10.1016/j.marpetgeo.2016.08.024.

Guo, X., Liu, K., Jia, C., et al., 2016c. Constraining tectonic compression processes by reservoir pressure evolution: overpressure generation and evolution in the Kelasu Thrust Belt of Kuqa Foreland Basin, NW China. Mar. Petrol. Geol. 72, 30–44. https://doi.org/10.1016/j.marpetgeo.2016.01.015.

Hao, F., Zou, H., Gong, Z., et al., 2007. Hierarchies of overpressure retardation of organic matter maturation: case studies from petroleum basins in China. AAPG Bull. 91 (10), 1467–1498. https://doi.org/10.1306/05210705161.

Hart, B.S., Flemings, P.B., Deshpande, A., 1995. Porosity and pressure: Role of compaction disequilibrium in the development of geopressures in a Gulf Coast Pleistocene basin. Geology 23 (1), 45–48. https://doi.org/10.1130/0091-7613(1995)023<0045:PAPROC>2.3.CO;2.

Hassanzadegan, A., Blöcher, G., Milsch, H., et al., 2014. The effects of temperature and pressure on the porosity evolution of flechtinger sandstone. Rock Mech. Rock Eng. 47 (2), 421–434. https://doi.org/10.1007/s00603-013-0401-z.

Huang, B., Piper, J.D.A., Peng, S., et al., 2006. Magnetostratigraphic study of the Kuche Depression, Tarim Basin, and Cenozoic uplift of the Tian Shan range, western China. Earth Planet Sci. Lett. 251 (3–4), 346–364. https://doi.org/10.1016/j.epsl.2006.09.020.

Jia, C., Gu, J., Zhang, G., 2002. Geological constraints of giant and medium-sized gas fields in Kuqa Depression. Chin. Sci. Bull. 47 (1), 47–54. https://doi.org/10.1007/BF02902818.

Ju, W., Hou, G., Zhang, B., 2014. Insights into the damage zones in fault-bend folds from geomechanical models and field data. Tectonophysics 610, 182–194. https://doi.org/10.1016/j.tecto.2013.11.022.

Lai, J., Li, D., Bai, T., et al., 2023. Reservoir quality evaluation and prediction in ultra-deep tight sandstones in the Kuqa Depression, China. J. Struct. Geol. 170, 104850. https://doi.org/10.1016/j.jsg.2023.104850.

Lai, J., Li, D., Wang, G., et al., 2019. Earth stress and reservoir quality evaluation in high and steep structure: The Lower Cretaceous in the Kuqa Depression, Tarim Basin. China. Mar. Petrol. Geol. 101, 43–54. https://doi.org/10.1016/j.marpetgeo.2018.11.036.

Lai, J., Su, Y., Xiao, L., et al., 2024. Application of geophysical well logs in solving geologic issues: Past, present and future prospect. Geosci. Front. 15 (3), 101779. https://doi.org/10.1016/j.gsf.2024.101779.

Lai, J., Wang, G., Chai, Y., et al., 2017. Deep burial diagenesis and reservoir quality evolution of high-temperature, high-pressure sandstones: Examples from Lower Cretaceous Bashijiqike Formation in Keshen area, Kuqa Depression, Tarim Basin of China. AAPG Bull. 101 (6), 829–862. https://doi.org/10.1306/08231614008.

Lai, J., Wang, G., Fan, Q., et al., 2022. Geophysical well-log evaluation in the era of unconventional hydrocarbon resources: A review on current status and prospects. Surv. Geophys. 43 (3), 913–957. https://doi.org/10.1007/s10712-022-09705-4.

Lai, J., Wang, G., Wang, S., et al., 2018. Review of diagenetic facies in tight sandstones: Diagenesis, diagenetic minerals, and prediction via well logs. Earth Sci. Rev. 185, 234–258. https://doi.org/10.1016/j.earscirev.2018.06.009.

Lai, J., Xiao, L., Song, X., et al., 2026. Mechanism of reservoir property variations in deep and ultra-deep sandstones in the Kuqa Depression, China. J. Asian Earth Sci. 309, 107150. https://doi.org/10.1016/j.jseaes.2026.107150.

Laubach, S.E., Zeng, L., Hooker, J.N., et al., 2023. Deep and ultra-deep basin brittle deformation with focus on China. J. Struct. Geol. 175, 104938. https://doi.org/10.1016/j.jsg.2023.104938.

Li, D., Wang, G.W., Bie, K., et al., 2025. Formation mechanism and reservoir quality evaluation in tight sandstones under a compressional tectonic setting: The Jurassic Ahe Formation in Kuqa Depression, Tarim Basin, China. Pet. Sci. 22 (3), 998–1020. https://doi.org/10.1016/j.petsci.2024.12.026.

Li, J., Wang, R., Qin, S., et al., 2024. Evolution of Mesozoic paleo-uplifts and differential control on sedimentation on the southern margin of Kuqa Depression, Tarim Basin. Mar. Petrol. Geol. 161, 106707. https://doi.org/10.1016/j.marpetgeo.2024.106707.

Liu, G., Yin, H., Lan, Y., et al., 2020. Experimental determination of dynamic pore-throat structure characteristics in a tight gas sandstone formation with consideration of effective stress. Mar. Petrol. Geol. 113, 104170. https://doi.org/10.1016/j.marpetgeo.2019.104170.

Luthi, S.M., Souhaite, P., 1990. Fracture apertures from electrical borehole scans. Geophysics 55 (7), 821–833. https://doi.org/10.1190/1.1442896.

Mahanta, B., Vishal, V., Sirdesai, N., et al., 2021. Progressive deformation and pore network attributes of sandstone at in-situ stress states using computed tomography. Eng. Fract. Mech. 252, 107833. https://doi.org/10.1016/j.engfracmech.2021.107833.

Meyer, G.G., Shahin, G., Cordonnier, B., et al., 2024. Permeability partitioning through the brittle-to-ductile transition and its implications for supercritical geothermal reservoirs. Nat. Commun. 15, 7753. https://doi.org/10.1038/s41467-024-52092-0.

Molnar, P., Tapponnier, P., 1975. Cenozoic tectonics of Asia: Effects of a continental collision: Features of recent continental tectonics in Asia can be interpreted as results of the India-Eurasia collision. Science 189 (4201), 419–426. https://doi.org/10.1126/science.189.4201.419.

Najibi, A.R., Ghafoori, M., Lashkaripour, G.R., et al., 2017. Reservoir geomechanical modeling: In-situ stress, pore pressure, and mud design. J. Petrol. Sci. Eng. 151, 31–39. https://doi.org/10.1016/j.petrol.2017.01.045.

Nikolinakou, M.A., Flemings, P.B., Gao, B., et al., 2023. The evolution of pore pressure, stress, and physical properties during sediment accretion at subduction zones. J. Geophys. Res. Solid Earth 128 (6), e2022JB025504. https://doi.org/10.1029/2022JB025504.

Obradors-Prats, J., Rouainia, M., Aplin, A.C., et al., 2017. Hydromechanical modeling of stress, pore pressure, and porosity evolution in fold-and-thrust belt systems. J. Geophys. Res. Solid Earth 122 (11), 9383–9403. https://doi.org/10.1002/2017JB014074.

Osborne, M.J., Swarbrick, R.E., 1997. Mechanisms for generating overpressure in sedimentary basins: A reevaluation. AAPG Bull. 81 (6), 1023–1041. https://doi.org/10.1306/522B49C9-1727-11D7-8645000102C1865D.

Ozkan, A., Cumella, S.P., Milliken, K.L., et al., 2011. Prediction of lithofacies and reservoir quality using well logs, Late Cretaceous Williams Fork Formation, Mamm Creek field, Piceance Basin, Colorado. AAPG Bull. 95 (10), 1699–1723. https://doi.org/10.1306/01191109143.

Screaton, E., Saffer, D., Henry, P., et al., 2002. Porosity loss within the underthrust sediments of the Nankai accretionary complex: Implications for overpressures. Geology 30 (1), 19–22. https://doi.org/10.1130/0091-7613(2002)030<0019:PLWTUS>2.0.CO;2.

Siggins, A.F., Dewhurst, D.N., 2003. Saturation, pore pressure and effective stress from sandstone acoustic properties. Geophys. Res. Lett. 30 (2), 1089. https://doi.org/10.1029/2002GL016143.

Spinelli, G.A., Mozley, P.S., Tobin, H.J., et al., 2007. Diagenesis, sediment strength, and pore collapse in sediment approaching the Nankai trough subduction zone. Geol. Soc. Am. Bull. 119 (3–4), 377–390. https://doi.org/10.1130/B25920.1.

Stricker, S., Jones, S. J. 2018. Enhanced porosity preservation by pore fluid overpressure and chlorite grain coatings in the Triassic Skagerrak, Central Graben, North Sea, UK. In: Armitage, P.J., Butcher, A.R., Churchill, J.M., et al. (Eds.), Reservoir Quality of Clastic and Carbonate Rocks: Analysis, Modelling and Prediction. Geological Society, London, Special Publications, vol. 435, pp. 321–341. https://doi.org/10.1144/SP435.4.

Su, Y., Lai, J., Dang, W., et al., 2024. Pore structure characterization and reservoir quality prediction in deep and ultra-deep tight sandstones by integrating image and NMR logs. J. Asian Earth Sci. 272, 106232. https://doi.org/10.1016/j.jseaes.2024.106232.

Su, Y., Lai, J., Dang, W., et al., 2026. Geological factors and fracture distribution in deep and ultra-deep sandstones in Kuqa Depression, Tarim Basin, China. Solid Earth 17 (4), 643–664. https://doi.org/10.5194/se-17-643-2026.

Sun, S., Hou, G., Zheng, C., 2017. Fracture zones constrained by neutral surfaces in a fault-related fold: Insights from the Kelasu tectonic zone, Kuqa Depression. J. Struct. Geol. 104, 112–124. https://doi.org/10.1016/j.jsg.2017.10.005.

Terzaghi, K., 1923. The calculation of the permeability coefficient of clay from the course of hydrodynamic stress phenomena [Die Berechnung der Durchlässigkeitsziffer des Tones aus dem Verlauf der hydrodynamischen Spannungserscheinungen]. Sitzungsberichte der Akademie der Wissenschaften in Wien, Mathematisch-Naturwissenschaftliche Klasse. Abteilung IIa 132, 125–138.

Towler, B.F., 2002. Fundamental Principles of Reservoir Engineering. Society of Petroleum Engineers. https://doi.org/10.2118/9781555630928.

Townend, J., Zoback, M.D., 2000. How faulting keeps the crust strong. Geology 28 (5), 399–402. https://doi.org/10.1130/0091-7613(2000)28<399:HFKTCS>2.0.CO;2.

Wang, B., Qiu, N., Amberg, S., et al., 2022. Modelling of pore pressure evolution in a compressional tectonic setting: The Kuqa Depression, Tarim Basin, northwestern. China. Mar. Petrol. Geol. 146, 105936. https://doi.org/10.1016/j.marpetgeo.2022.105936.

Wang, J.P., Zeng, L.B., Zhou, L., et al., 2023. Development model of natural fractures in ultra-deep sandstone reservoirs with low porosity in Kelasu tectonic belt, Tarim Basin. Earth Sci. 48 (7), 2520–2534. https://doi.org/10.3799/dqkx.2022.138 (in Chinese).

Wang, M., Chen, Y., Bain, W.M., et al., 2020a. Direct evidence for fluid overpressure during hydrocarbon generation and expulsion from organic-rich shales. Geology 48 (4), 374–378. https://doi.org/10.1130/G46650.1.

Wang, W., Yin, H., Jia, D., et al., 2020b. Along-strike structural variation in a salt-influenced fold and thrust belt: analysis of the Kuqa Depression. Tectonophysics 786, 228456. https://doi.org/10.1016/j.tecto.2020.228456.

Wei, G., Zhao, Z., Zhang, R., et al., 2026. Fracture-pore networks and brittle with ductile stress-strain mechanisms: Triaxial tests on >7,600 m samples yield insights for 10,000-m deep sandstones. Sci. China Earth Sci. 69, 702–720. https://doi.org/10.1007/s11430-025-1776-8.

Xi, K., Cao, Y., Haile, B.G., et al., 2021. Diagenetic variations with respect to sediment composition and paleo-fluids evolution in conglomerate reservoirs: A case study of the Triassic Baikouquan Formation in Mahu Sag, Junggar Basin, northwestern China. J. Petrol. Sci. Eng. 197, 107943. https://doi.org/10.1016/j.petrol.2020.107943.

Yang, H.J., Shi, W.Z., Du, H., et al., 2024b. Hydrocarbon charging periods and maturities in Bozi-Dabei area of Kuqa Depression and their indications to the structural trap sequence. Acta Pet. Sin. 45 (10), 1480–1491 (in Chinese).

Yang, K., Qi, J., Xu, L., et al., 2024a. Influence of preexisting structures on salt structures in the Kuqa Depression, Tarim Basin, Western China: insights from seismic data and numerical simulations. Basin Res. 36, e12850. https://doi.org/10.1111/bre.12850.

Yu, S., Chen, W., Evans, N.J., et al., 2014. Cenozoic uplift, exhumation and deformation in the north Kuqa Depression, China as constrained by (U–Th)/He thermochronometry. Tectonophysics 630, 166–182. https://doi.org/10.1016/j.tecto.2014.05.021.

Zeng, L., Jiang, J., Yang, Y., 2010. Fractures in the low porosity and ultra-low permeability glutenite reservoirs: A case study of the late Eocene Hetaoyuan Formation in the Anpeng Oilfield, Nanxiang Basin. China. Mar. Petrol. Geol. 27 (7), 1642–1650. https://doi.org/10.1016/j.marpetgeo.2010.03.009.

Zeng, L., Song, Y., Liu, G., et al., 2023. Natural fractures in ultra-deep reservoirs of China: A review. J. Struct. Geol. 175, 104954. https://doi.org/10.1016/j.jsg.2023.104954.

Zeng, Q., Mo, T., Zhao, J., et al., 2020. Characteristics, genetic mechanism and oil & gas exploration significance of high-quality sandstone reservoirs deeper than 7000 m: A case study of the Bashijiqike Formation of Lower Cretaceous in the Kuqa Depression, NW China. Nat. Gas Ind. B 7 (4), 317–327. https://doi.org/10.1016/j.ngib.2020.01.003.

Zhang, J., 2011. Pore pressure prediction from well logs: Methods, modifications, and new approaches. Earth Sci. Rev. 108 (1–2), 50–63. https://doi.org/10.1016/j.earscirev.2011.06.001.
Zhang, J., Hüpers, A., Kreiter, S., et al., 2021. Pore pressure regime and fluid flow processes in the shallow Nankai Trough subduction zone based on experimental and modeling results from IODP site C0023. J. Geophys. Res. Solid Earth 126 (2), e2020JB020248. https://doi.org/10.1029/2020JB020248.
Zhang, Z., Tang, P., Sun, J., et al., 2024. Chronology, structures and salt tectonics in the northern Kuqa Depression, NW China: Implications for the Cenozoic uplift of Tian Shan and foreland deformation. Global Planet. Change 243, 104618. https://doi.org/10.1016/j.gloplacha.2024.104618.
Zhao, F., Lai, J., Xia, Z.L., et al., 2025a. Coaly source rock evaluation using well logs: The Jurassic Kezilenuer formation in Kuqa Depression, Tarim Basin, China. Pet. Sci. 22 (9), 3599–3612. https://doi.org/10.1016/j.petsci.2025.05.029.
Zhao, G., Guo, Y., Yang, C., et al., 2025b. Effect of temperature and pressure on mechanical behavior of reservoir shales at different depths: implications for deep shale gas extraction. Rock Mech. Rock Eng. 58 (6), 6169–6194. https://doi.org/10.1007/s00603-025-04470-3.
Zoback, M.L., 1992. First- and second-order patterns of stress in the lithosphere: the world stress map project. J. Geophys. Res. 97 (B8), 11703–11728. https://doi.org/10.1029/92JB00132.